SURF Final Report
September 28, 2006

Angular Noise in a Suspended Interferometer with DC Readout

Royal Reinecke
Mentor: Alan Weinstein
Co-Mentor: Rana Adhikari

Abstract

In the LIGO interferometers, optical levers are used to monitor and control the angular motion of the suspended mirrors. Optical lever servos are essential for establishing or regaining lock, so the better they perform, the faster lock can be achieved, thereby increasing the total amount of time that useful data can be taken. The work here deals with characterizing the various sources of noise in the optical levers at the 40 meter prototype interferometer at Caltech. It studies the optical lever noise at the 40 m due to mirror motion induced by the servo as it feeds back on seismic noise, electronic noise, and noise due to optical lever laser intensity fluctuations. This information can be used to determine the contributions of the various noise sources to the total angular noise floor under the proposed DC readout scheme being prototyped at the 40 m for use in Advanced LIGO. We can then reduce the dominant sources and so decrease the noise level of the optical lever system, thus lowering its contribution to the overall interferometer noise budget.

Introduction

Stationary gravitational fields can be described through general relativity as curvature in space-time. The more massive an object is, the greater the curvature. This leads to phenomena such as gravitational lensing, in which light bends around massive objects such as galaxies.

Gravity waves occur due to changes in gravitational fields from accelerating masses. If one mass moves with respect to another at some frequency, then a gravitational wave propagates outward carrying energy with it. As curvature changes due to changing fields, so do distances in space-time. However, this effect is typically very minute, and so it can be difficult to observe due to many noise sources of greater amplitude. Observed strain increases with the mass of objects involved and with their velocities and so astrophysical sources are the best for study.

Like electromagnetic waves, gravitational waves are transverse and travel at the speed of light. However, instead of by photons, gravity waves propagate by means of massless spin-2 particles called gravitons. The spin of two comes from the fact that an accelerating mass can be thought of as having a quadrupole moment, and quadrupoles have a spin of 2. Basically from one moment to the next, space stretches and squishes transverse to the direction in which the waves propagate. Waves of larger amplitude lead to greater strain h, where h is given by $\Delta L/L$. When a gravity wave travels by polarized

along one arm of an interferometric observatory with two orthogonal arms of length L, one arm will grow in length by ΔL while the other will shrink by ΔL.

The search for gravitational waves has developed into an international network of interferometric and bar detectors. The interferometers use the invariance of the speed of light to detect differential motion between the two arms.

The LIGO project in the United States has three detectors, two in Hanford, Washington and one in Livingston, Louisiana. All of LIGO's interferometers use the same basic setup which consists of a Michelson interferometer with Fabry-Perot cavities along the arms which store light, effectively lengthening the arms. The configuration for Advanced LIGO can be seen in Figure 1.

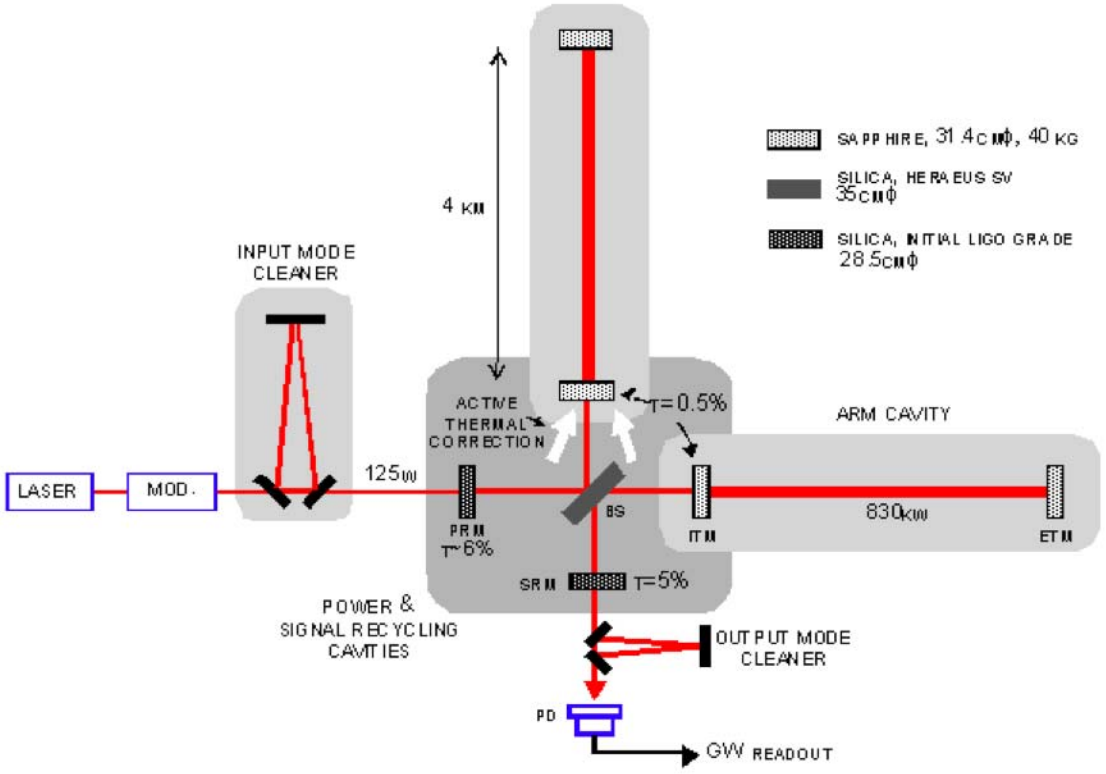

Figure 1: Advanced LIGO Configuration.

When trying to detect strains on the order of 10^{-21}, noise must be very carefully controlled. The interferometers of LIGO have reached the point where they are no longer limited by technical sources of noise, but now by fundamental noise sources, specifically seismic, thermal, and quantum.

Characterizing the Noise in the Optical Lever System at the 40m Prototype Interferometer

The 40 meter interferometer at Caltech serves as a prototype for Advanced LIGO. Research carried out at this facility deals with improving methods of lock acquisition and testing new hardware including electronics and optical layouts that may be put into place in Advanced LIGO. In particular, a new DC readout beamline is under construction this the summer. The 40m also has a signal cavity with a signal recycling mirror. Other people in the lab are working on the 40m noise budget, input mode cleaner enhancements, a new output mode cleaner design, improving wavefront sensors, and developing squeezed vacuum.

The work described here deals with characterizing the various sources of noise in the optical levers. This will be important for reducing the overall displacement noise level of the interferometer, especially when the new DC readout detection scheme is in place.

At the sites, the optical levers are used for establishing or regaining lock, so the better they perform, the faster lock can be achieved thereby increasing the total amount of time that useful data can be taken. After lock is attained, they are also used to stabilize the optic jitter from .5 to 2 Hz, while the more accurate wavefront sensors are used to control the positions of the mirrors at all frequencies. At present, the 40 m interferometer does not have wavefront sensors, so the optical lever system plays an important role in controlling the angular positions of the mirrors while the interferometer is in lock and even when it is not.

Here we report on the study of the optical lever noise at the 40 m due to angular mirror motion caused by seismic noise, electronic noise, shot noise, and noise due to optical lever laser intensity fluctuations.

Another source of noise, which limits sensitivity at the sites but cannot yet be seen at the 40m, is laser angular jitter. Movement of the optical lever lasers cannot be distinguished from actual angular motion of the mirrors. In addition to characterizing noise in the optical levers of the prototype interferometer, we also report on the development of designs for advanced LIGO to reduce laser jitter noise.

The 40 m Interferometer

The 40 m interferometer is basically a Michelson interferometer with Fabry Perot arm cavities as seen in Figure 2. There are seven main mirrors, each with an optical lever to sense angular mirror motion in pitch (top to bottom tilt) and yaw (side to side tilt). The optical levers are shown in the diagram. Each one basically consists of a laser bouncing off a mirror and onto a QPD. The longer the lever arm is, the more sensitive the optical lever can be.

At the center of the interferometer is a beam splitter (BS), that splits the laser light equally down the two arms. Each arm (X, Y) has a flat initial test mass (ITM), and spherically curved end test mass (ETM). Additionally there is a power recycling mirror (PRM) to increase the laser power in the setup. Though not shown on this picture, there is also a signal recycling mirror (SRM) before the asymmetric port that will be used to extract the gravitational wave signals.

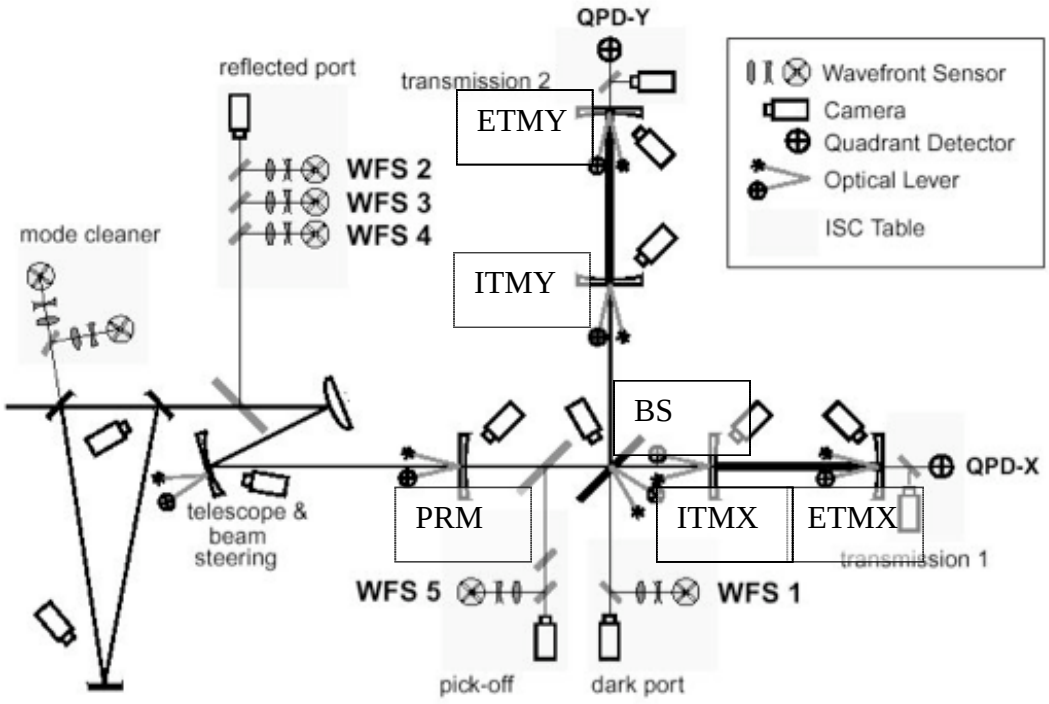

Figure 2: Interferometer Configuration with Optical Levers Shown

Figure 3 shows a schematic of a suspended optic. There are four magnets on the face of the mirror and one on the side. The coils in the sensor/actuator heads (OSEMs) drive the magnets in order to control the motion of the mirror in all degrees of freedom.

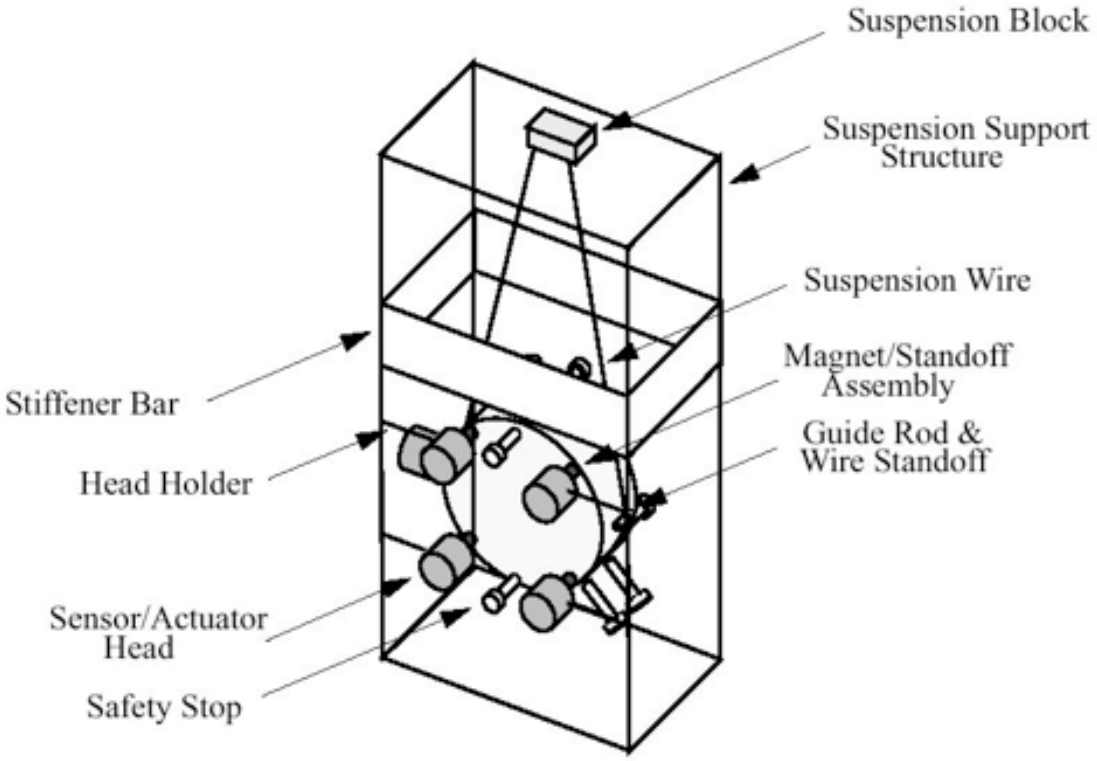

Figure 3: Suspended Optic

A detailed view of the OSEM can be seen in Figure 4. The LED/photodiode pair senses motion while the coil pushes and pulls on the magnet against pendulum motion of the test mass.

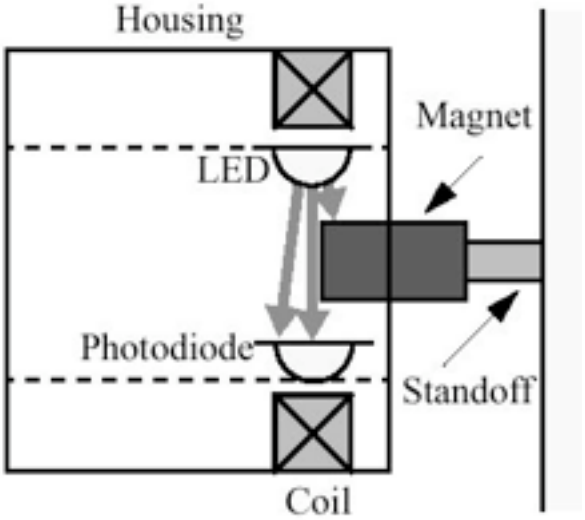

Figure 4: OSEM

Here we examine only the oplevs for the four test masses (ITMX, ETMX, ITMY, ETMY) and not the other three mirrors (BS, PRM, SRM), since the former dominate overall interferometer noise on account of the high-finesse arms.

Tilts of the test masses lead to angular and translational displacements of the arm cavity axes, which show up as noise at the dark port because the jitter causes the power going through the OMC to fluctuate and the DC readout is sensitive to direct power fluctuations. In this way mirror tilts couple to overall interferometer noise since the power fluctuations they cause at the dark port show up as apparent DARM signals, or false gravitational waves.

Figure 5 and Figure 6 show the residual jitter (error signals) seen by the optical lever sensors for the four test masses at the beginning of the summer. The absolute scale of mirror tilt on the y-axis was calibrated using the method in Appendix A. The data on these two plots seem to show actual mirror motion below about ten hertz, but then reach a noise floor of approximately 10^{-9} radians out to high frequencies where the mirrors cannot move that fast. This discrepancy called for a detailed analysis of possible noise sources. Though not shown on these plots, the RMS values of the data are contained in the xml files and can be compared to rms values of data taken after future noise improvements in the optical lever system.

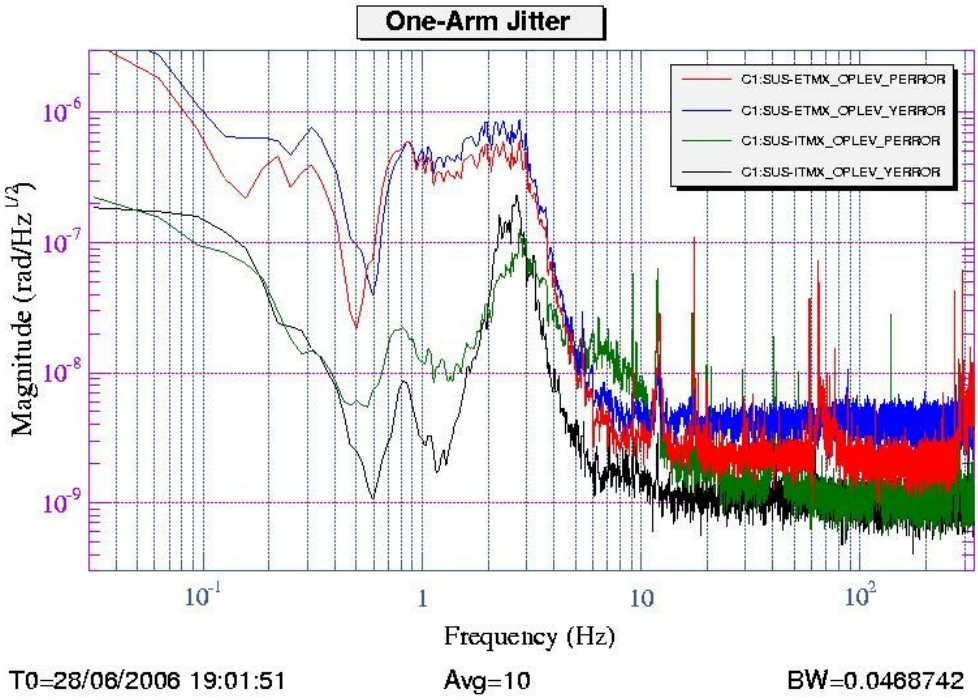

Figure 5: Initial X Arm Jitter Seen by Optical Levers.

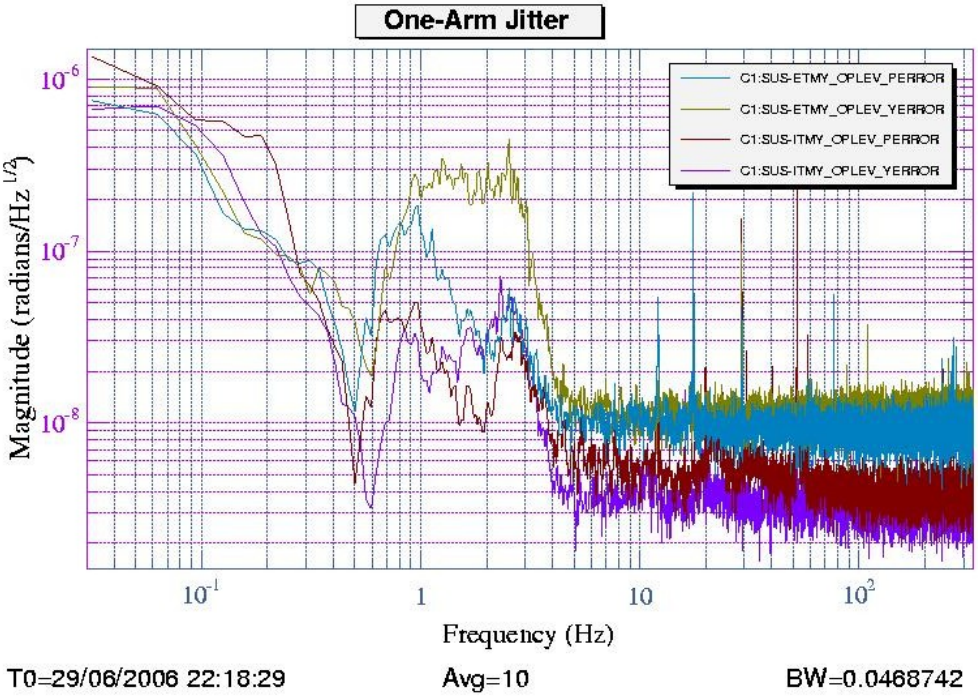

Figure 6: Initial Y Arm Jitter Seen by Optical Levers.

Mirror Motion due to Servo

As the servo attempts to hold the mirrors in place at low frequencies by feeding back on the error signals (representing mirror tilts), it also causes them to move by introducing noise at high frequencies. At the beginning of the summer, it was found that electronic noise dominated the error signal plots above a few hertz. Thus the servo overcompensates for false mirror motion signals by applying extra force at frequencies above about 10 hertz.

At low frequencies where mirror motion is relatively large, the oplev sensors are reliable, so one can use the tilt error signals to determine the true mirror angular displacements. At high frequencies, where mirror motion is small, the oplev sensors are insufficiently sensitive, and the mirror tilt is primarily induced by the forces applied by the servo as measured by the out signals.

Figure 7 shows the servo topology with the various signals labeled. Such a servo exists for the pitch and yaw signals of each mirror.

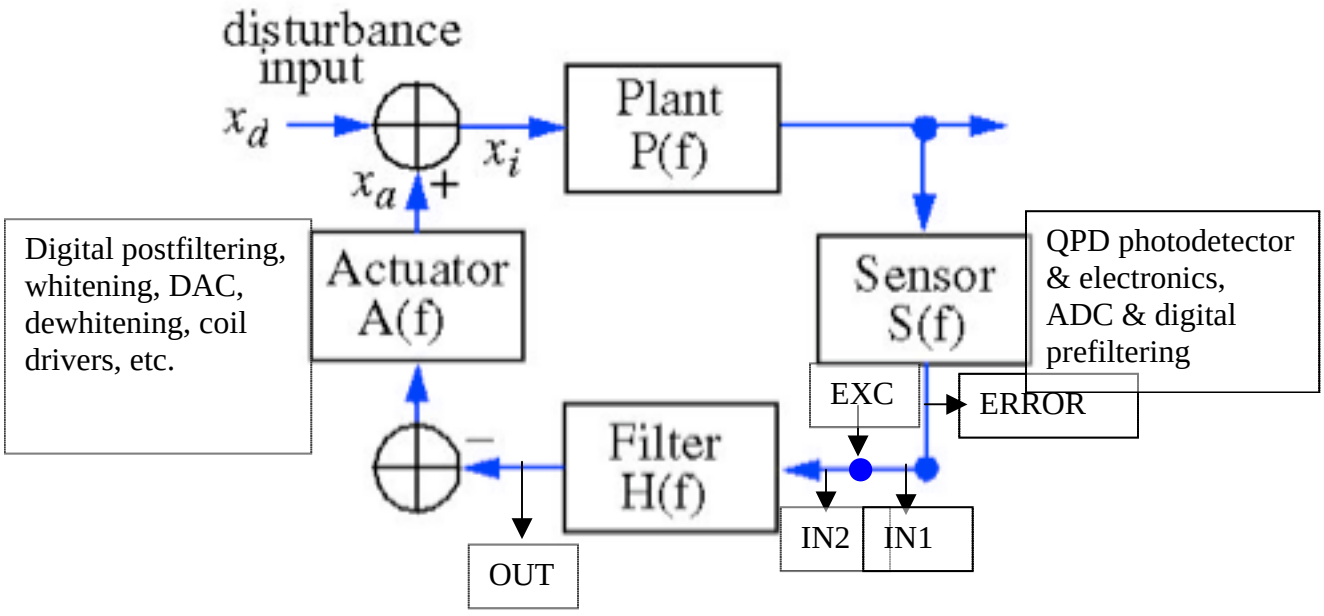

Figure 7: Servo Topology.

The optical lever "out" signals drive the coils and are thus proportional to the torque applied to the mirrors by the coils. Since torque, $\tau = I\ddot{\theta} = I\theta(2\pi f)^2$, where I is the moment of inertia, and $\ddot{\theta}$ is the angular acceleration of the mirror, the torque signal can be calibrated to the actual angular tilt signal of a mirror at a particular frequency f_0. Then this calibration factor can be scaled to other frequencies by $(f_0/f)^2$ to obtain the mirror displacement at different frequencies from the torque signal.

In fact the actual calibration I used to go from the out signal to an error signal was $outsignal \cdot \frac{error \text{ at } f_{cal}}{out \text{ at } f_{cal}} \cdot \frac{\left|f_0^2 + if_0 \cdot f_{cal}/Q - f_{cal}^2\right|}{\left|f_0^2 + if_0 \cdot f/Q - f^2\right|}$, where Q is the quality factor (3 in this case), f_0 is the resonant frequency (.5Hz for pitch and .6Hz for yaw), and f_{cal} is the frequency at which the calibration frequency was obtained (10Hz in all cases). We can then convert the error signals to radians of tilt of the mirrors using the calibration described in Appendix A.

The servo is applying forces to cancel the noisy motion of the mirrors at low frequencies so the torque signal reduces mirror motion instead of causing it. Thus the net mirror motion is less than what is shown in the servo figures below a few hertz.

Since mirror motion drops off tremendously at higher frequencies, this calibration tells us how much the mirror is really moving, without the false movement indicated by the directly measured tilt signals that are dominated by electronic noise at high frequencies.

Figure 8 and Figure 9 show the results for all four mirrors in pitch and yaw.

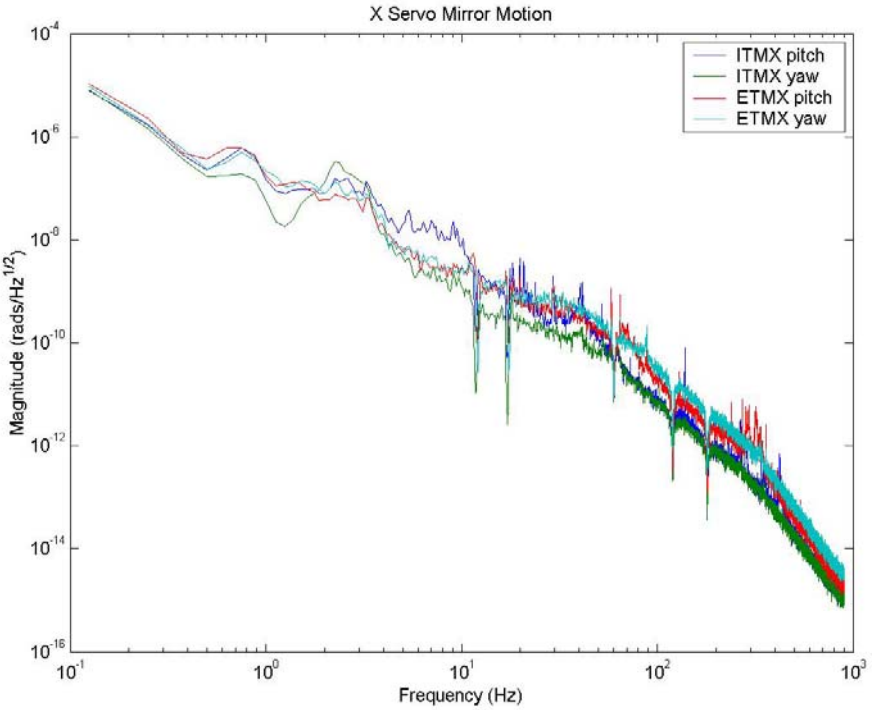

Figure 8: X Arm Mirror Motion Induced by Servo.

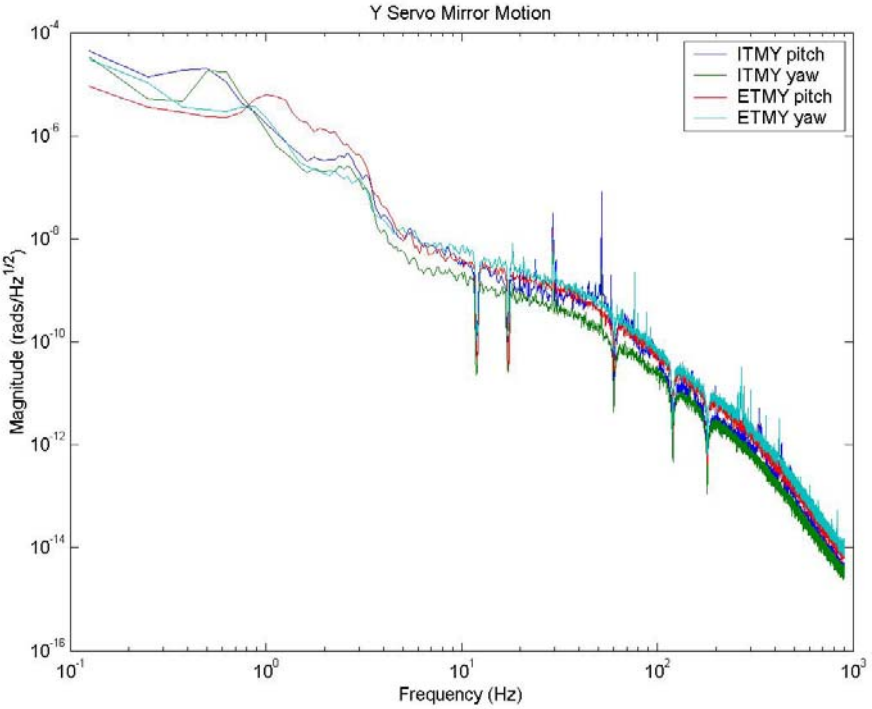

Figure 9: Y Arm Mirror Motion Induced by Servo.

Originally the servos used the elliptic 40 filter seen in blue on the plots in Figure 10. However, based on the calibrated spectra of noise induced by the servo, these filters were switched out and replaced by ELP35 filters (seen in red).

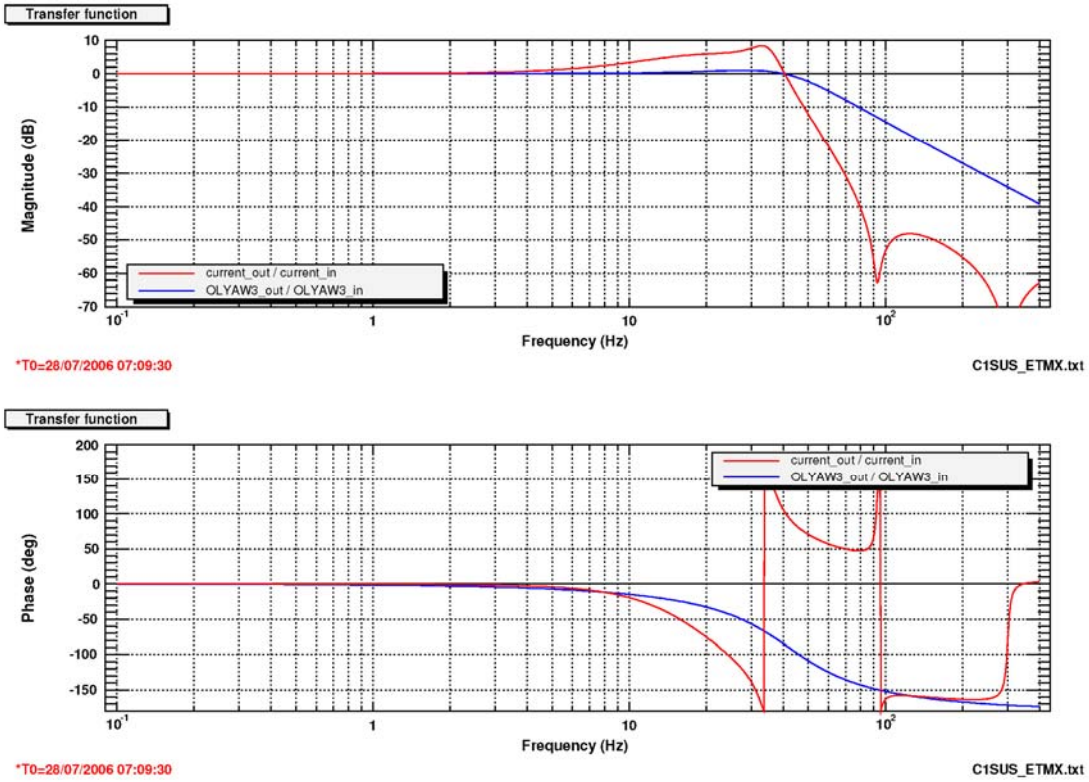

Figure 10: Comparison of ELP40 (blue) and ELP35 (red) Filters.

After applying the new filter, data were taken from the out channels as before. The effects can be seen in Figure 11 and Figure 12, where the reduction in [predicted] angular displacement noise in the frequency range between 30 and 1000 Hz is evident.

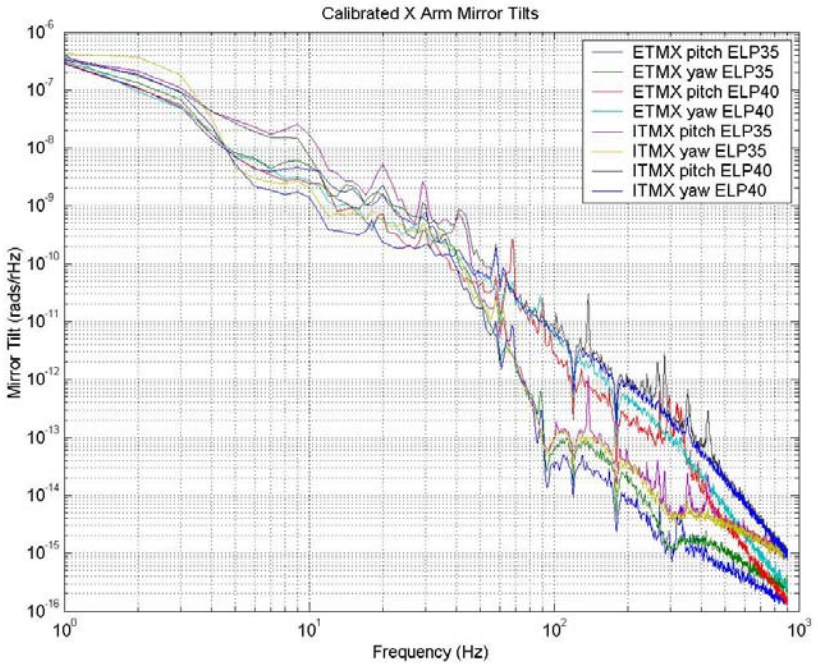

Figure 11: Effect of New Filter on X Arm Mirror Motion.

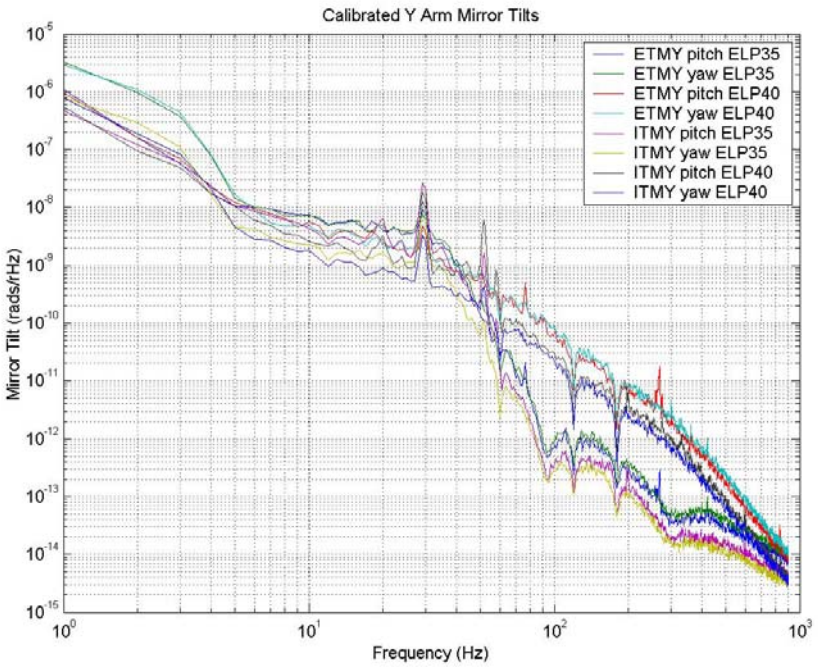

Figure 12: Effect of New Filter on Y Arm Mirror Motion.

While fixing the filters for the optical levers of the test masses, the new filters were also added to the optical levers for the beam splitter, power recycling mirror, and signal recycling mirrors with the following uncalibrated results.

Figure 13 shows the results for the beam splitter.

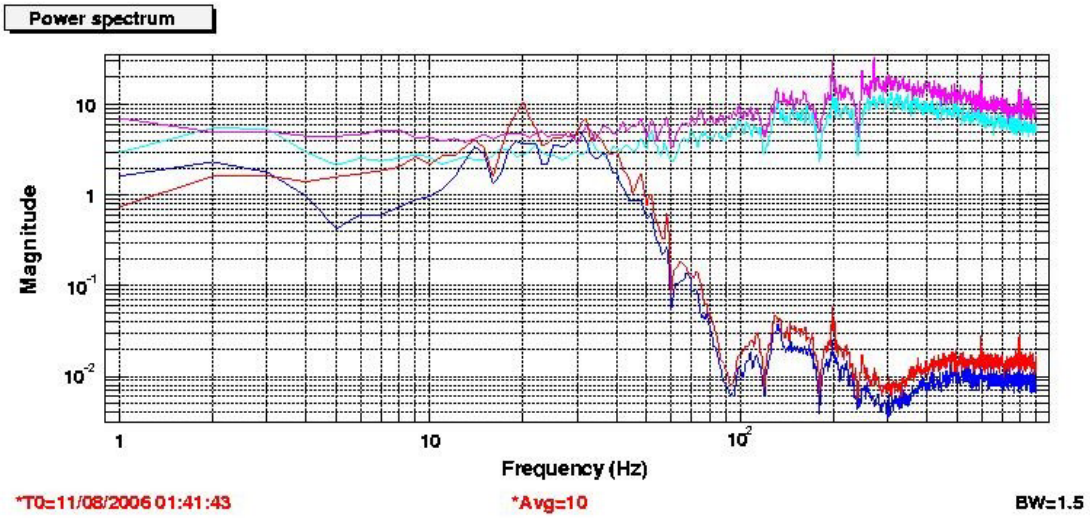

Figure 13: Effect of ELP35 Filter on Beam Splitter.

(Red-pout, Blue-yout, Magenta-old pout, Cyan-old yout)

Figure 14 shows the results for the power and signal recycling mirrors.

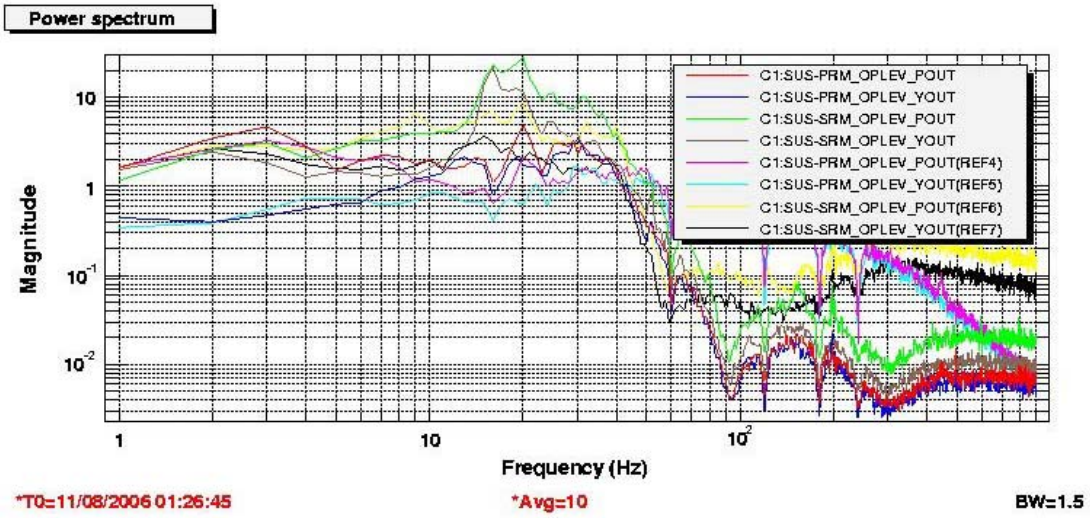

Figure 14: Effects of ELP35 on PRM and SRM.

Electronic Noise

Measuring the electronic noise proved very simple. The pitch and yaw signals for the four mirrors were measured with all four photodiodes uncovered and then with them all covered. Since pitch and yaw signals are divided by the quadrant sum, the spectra from the dark photodiodes were multiplied by the dark sum divided by the bright sum as read from the EPICS screens. This gives the pitch and yaw signals that would be seen if the beams were hitting the photodiodes but were not affected by any other motion of the mirrors, lasers, ground, etc. Of note, however, is the fact that the front end signals follow a different path than the EPICS signals, so the sums (especially when small as in the dark case) are different. Figure 15 and Figure 16 show that only ITMX has decent noise and that the other mirrors are all much worse. It also might be a calibration error that ETMX pitch and yaw do not have the same noise level.

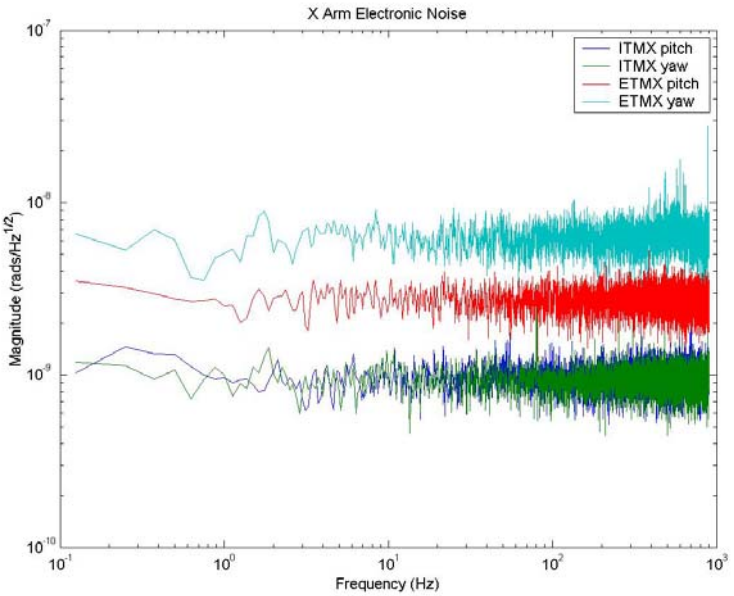

Figure 15: X Arm Electronic Noise

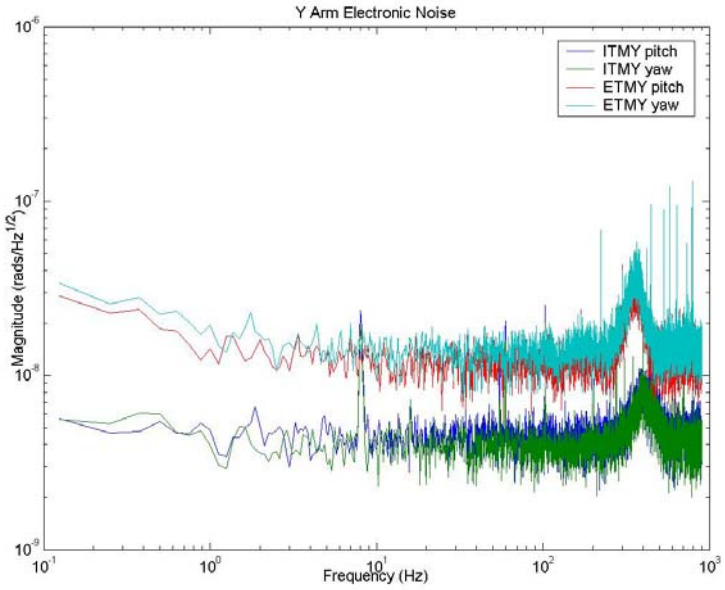

Figure 16: Y Arm Electronic Noise

The data are a little fuzzy, so it would be a good idea to retake them with more averages. Much of this electronic noise comes from analog to digital conversion of the signals. Electronic noise can be reduced by amplifying the actual signal before this step, and by then deamplifying it afterward. A good technique to use is to add whitening circuitry, which was done for the ETMX soon after these data were taken, though the other three mirrors seemed to be missing whitening boards.

Figure 17 shows the uncalibrated results that compare the whitened ETMX with the new ELP35 filter to the ETMY with the old filter and no whitening. The error signal plot (top) shows an electronic noise floor that is a factor of almost hundred lower than the signal without whitening (albeit from a different suspended optic) above 4 Hz. Of course, most of this improvement is due to the new filter, since the whitening only starts to have an effect well above 15 Hz.

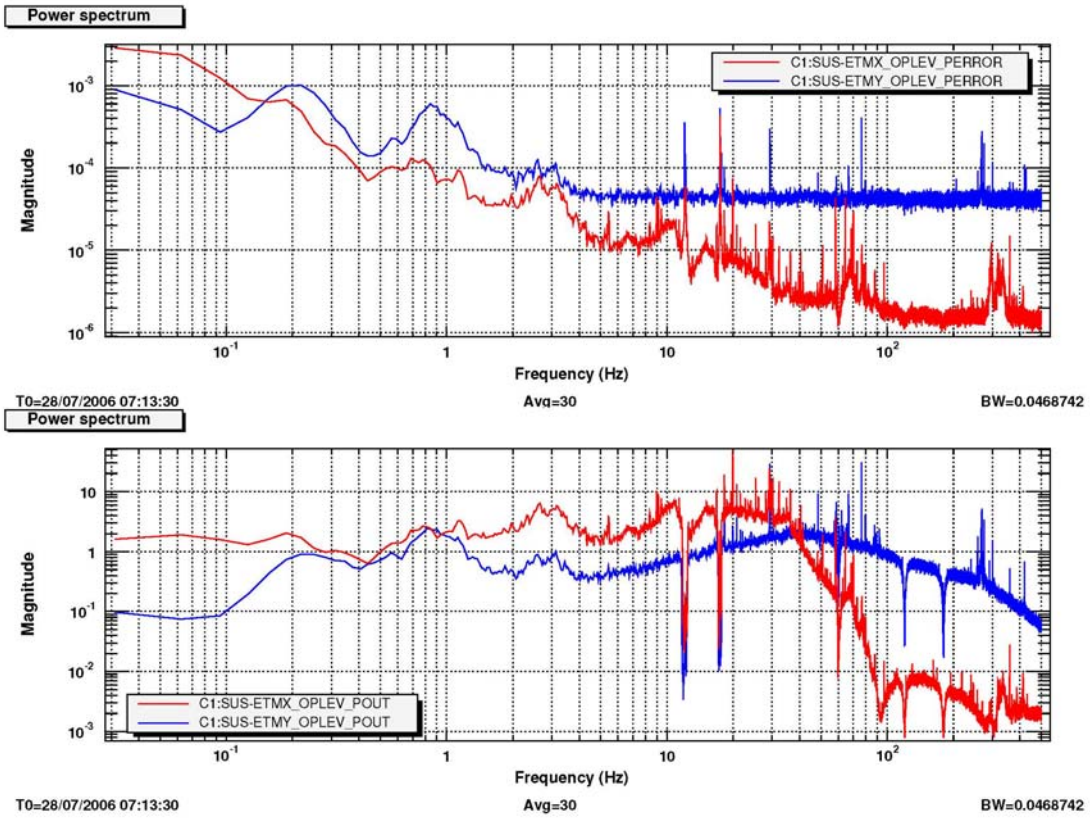

Figure 17: Effects of Whitening and ELP35 Filter on Error and Out Signals.

The whitening for the ETMX comes from the use of a Generic Pentek Input Board with a zero at 15 Hz and a pole at 150 Hz. Unfortunately this circuit is not tailored to the actual electronic noise of the optical levers. A new circuit was designed and constructed for the ETMY with a zero at 1 Hz and pole at 10 Hz that should significantly improve the electronic noise once it is inserted into the racks. A generic board was modified by soldering on new resistors in both whitening and lowpass filter stages. The lowpass filters had cutoff frequencies of just 800 Hz, but the sampling rate of the equipment goes up to 8192 Hz. Thus the new lowpass filters were set up to have –20 dB gain reduction at 8192 Hz. Similar filters can be constructed for the ITMX, ITMY, and ETMX. The electronic noise spectra and error signal spectra will be measured for all four test masses before and after these filters are installed.

Figure 18 shows the original circuit that the output of each quadrant of the optical lever QPDs would go through on the generic board.

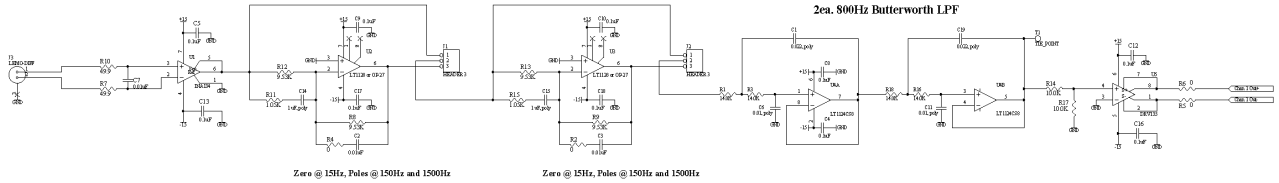

Figure 18: Generic Pentek Input Board Circuit.

Figure 19 shows a closeup of one of the whitening stages with the changes noted by the red arrows:

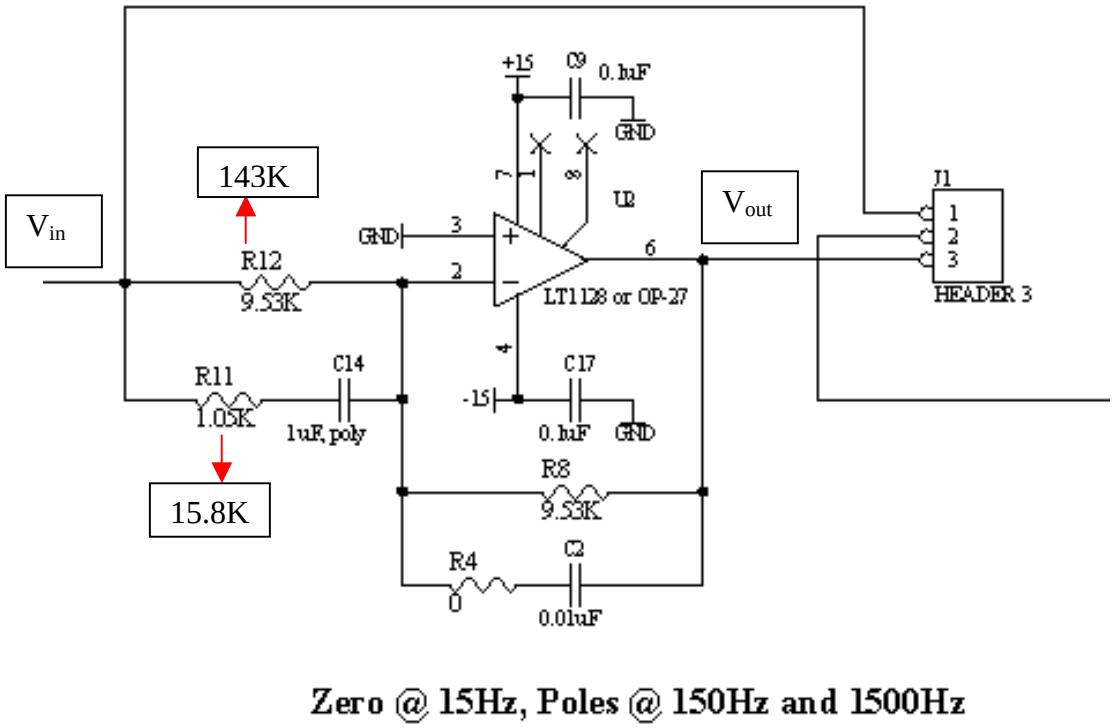

Figure 19: Whitening Stage.

For this circuit we have the transfer function given by:

$$\frac{V_{out}}{V_{in}} = \frac{R_8}{R_8 i\omega C_2 + 1} \cdot \frac{(R_{11} + R_{12}) i\omega C_{14}}{R_{11} R_{12} i\omega C_{14} + R_{12}}$$

This alteration means a zero at 1 Hz and poles at 10 Hz as well as 1500 Hz from before.

Figure 20 shows one of the original Sallen Key Butterworth Lowpass Filter stages with modifications shown:

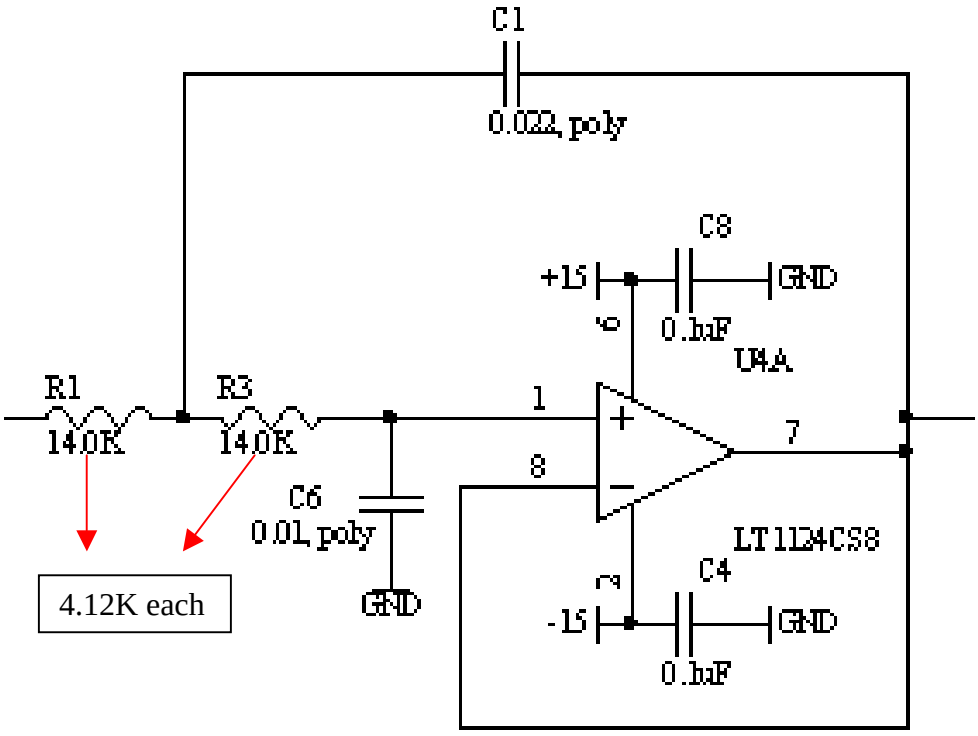

Figure 20: Butterworth Lowpass Filter.

The new cutoff frequency for this lowpass filter is at $f_c = \frac{1}{2\pi\sqrt{R_1 R_3 C_1 C_6}} = 2591\,\text{Hz}$.

Since the magnitude of the output divided by the input drops off as $1/f^2$ the gain is reduced by 20 dB at 8192 Hz.

Laser Intensity Noise

The optical lever laser diodes used at the 40 m are small $60 units (Part #31-0425-000) made by Coherent. The company does not advertise these lasers as having any noise reduction circuitry and does not provide information on the stability of the output power. Thus laser intensity fluctuations could be significant.

Fluctuations in optical lever laser intensity show up as false pitch and yaw signals. This is because pitch and yaw signals get divided by averaged quadrant sums. A spectrum analyzer and oscilloscope were used to determine the magnitude of the intensity fluctuations. Then the intensity noise was converted to pitch and yaw signals. To do this, a chopper was placed in front of the ITMX optical lever laser that made it possible to find the magnitude of pitch and yaw signals when intensity went from 0 to its max value as the chopper passed through the beam at 200 hertz. For the pitch measurement, the beam was sent through the chopper so that it passed through the top where the blades are vertical to avoid false pitch signals. Likewise for the yaw measurement, the beam passed through the chopper at the side where the blades are horizontal to avoid false yaw signals.

Figure 21 shows the tilt fluctuations given by the calibration:

Tilt fluctuations (rads/$Hz^{1/2}$) =
Intensity fluctuations (V/$Hz^{1/2}$) * Total tilt variation (rads) / DC Intensity (V)

In this case the intensity fluctuations were measured by a spectrum analyzer connected to a photodiode placed in the path of the oplev laser beam. (A dark spectrum was also taken and substracted from the bright one to get the actual fluctuations due to the laser and not the photodiode.) The DC intensity of the beam was measured with an oscilloscope with the same photodiode used to measure fluctuations in the same relative position to the laser. For example, the DC intensity of the ITMX oplev laser was 3.84 V;
total pitch variation (measured with DTT time series measurement of the 200Hz oscillations) was $[.026 \pm .004] cnts \times .000065 \frac{rads}{cnt} = [1.69 \pm .26] \times 10^{-6} rads$;
and total yaw variation (again measured by DTT time series) was
$[.024 \pm .004] cnts \times .000057 \frac{rads}{cnt} = [1.37 \pm .23] \times 10^{-6} rads$.

Comparison of noise due to the oplev lasers with the previous plots show that angular noise due to intensity fluctuations appears to be negligible. However, if we can get other noise sources down to the point where the intensity fluctuation noise becomes significant, it may be important to stabilize the laser intensity, or get better lasers.

Tilt fluctuations (rads/$Hz^{1/2}$) =
Intensity fluctuations (V/$Hz^{1/2}$) * Total tilt variation (rads) / DC Intensity (V)

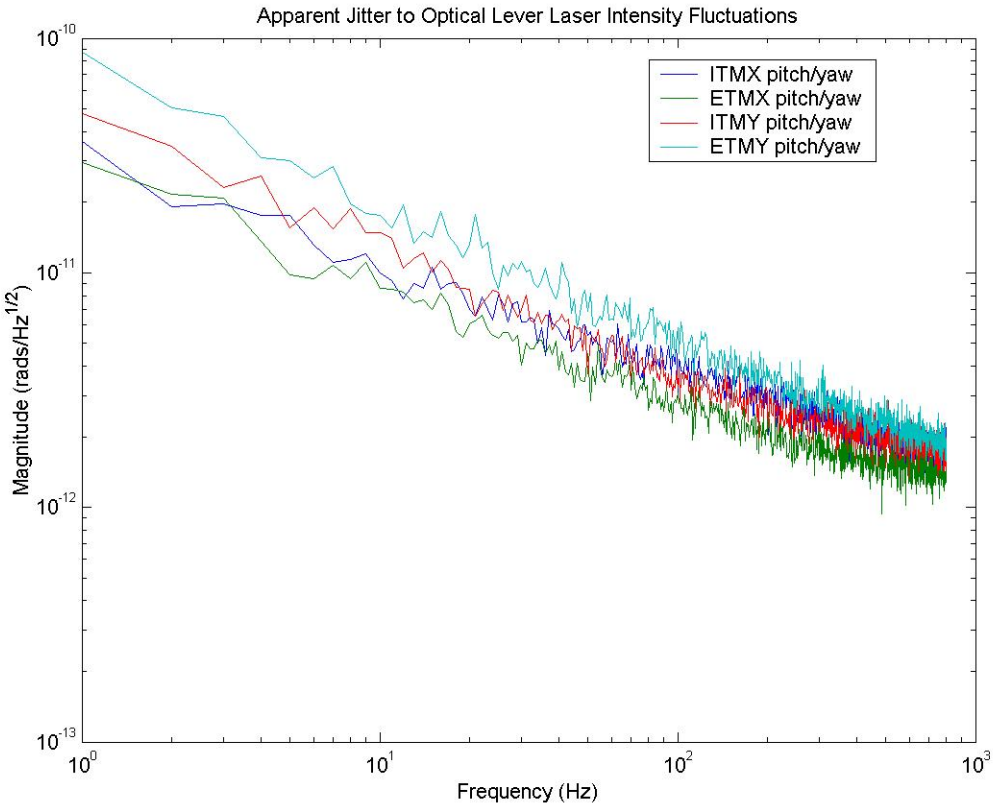

Figure 21: Laser Intensity Noise.

Inside of Optical Lever Laser Diode Module

After measuring the laser intensity fluctuations, it was necessary to find out what sort of circuitry the module contained before attempting to add any sort of noise reduction filter to the two input pins. Unfortunately the company would not disclose this proprietary information. Using a hacksaw to remove the casing from the diode module, it became possible to study the circuitry inside. Unfortunately the components are very small and rather more numerous than expected as seen in Figure 22 and Figure 23. This poses an obstacle to any efforts to add extra circuitry to reduce fluctuations in diode power output.

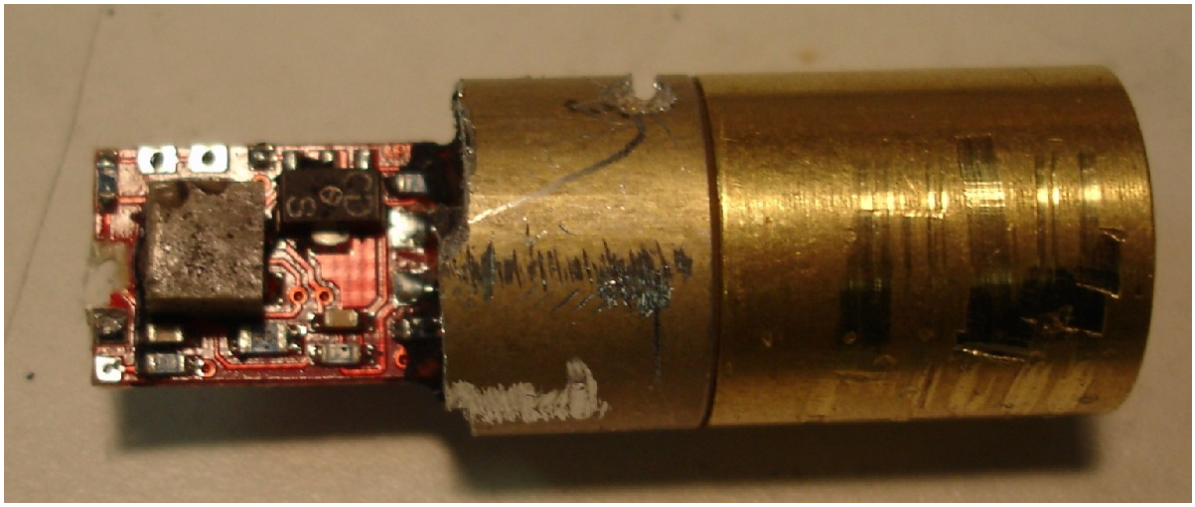

Figure 22: Inside Optical Lever Laser Diode Module.

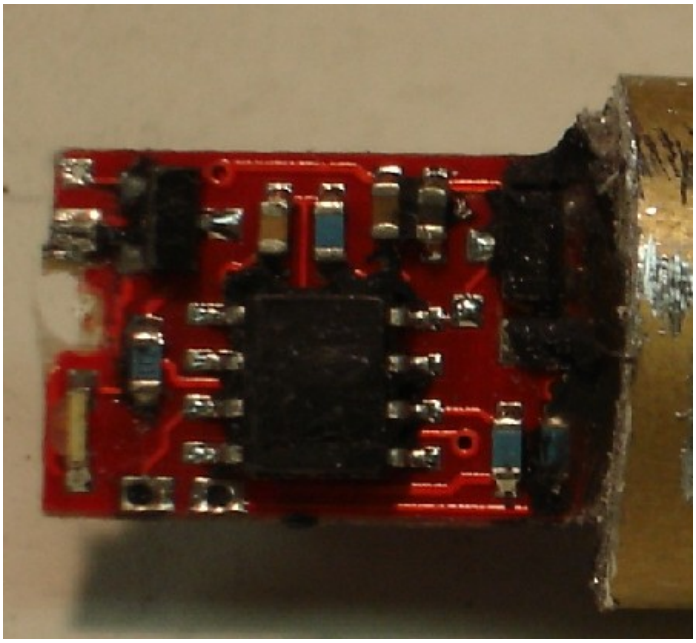

Figure 23: Close-up View of Other Side of Circuit Board.

Measurement of Optical Lever Laser Transfer Function

In order to reduce the influence of laser intensity fluctuations on the optical lever angular displacement measurement, we would like to be able to control the laser intensity by modulating the input current of the laser. To see whether this would work, a bias tee consisting of a 10mH inductor and a 47 microFarad capacitor was constructed. Then it was connected the three ends to a DC power supply at 60mA, a source signal generated by the spectrum analyzer, and the input current of the laser. The setup appears in Figure 24 and Figure 25.

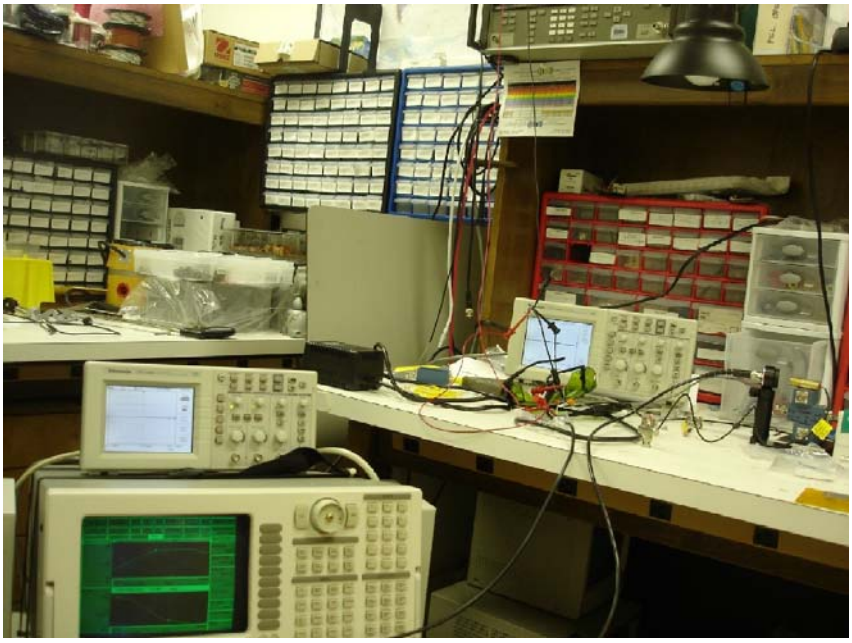

Figure 24: Experimental Setup.

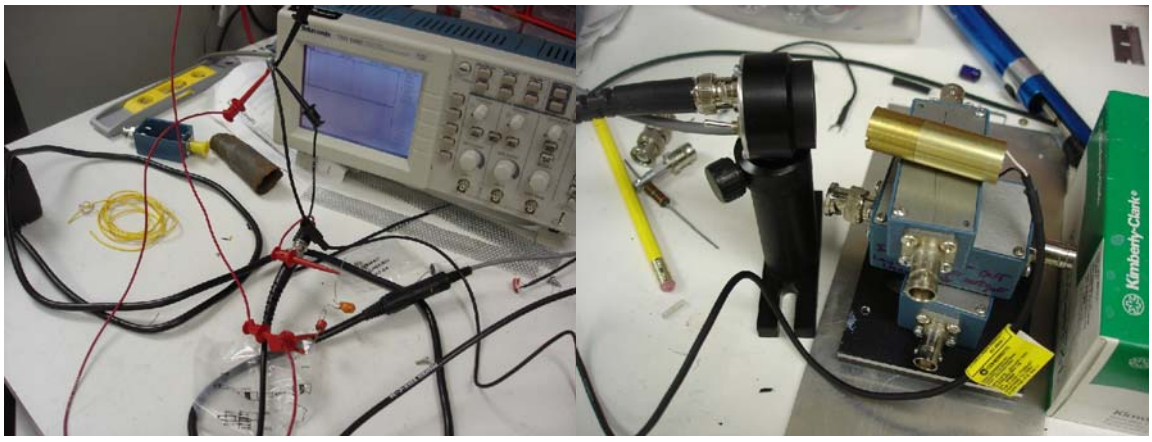

Figure 25: Bias Tee Circuit and Laser Aimed at Photodiode.

The spectrum analyzer was used to obtain the transfer function of pin voltage to diode power seen in Figure 26.

In theory the corner frequency should be at $\frac{1}{2\pi\sqrt{LC}}$ = 232 Hz. This value agrees with the data shown. You can also see a slight rolloff above 10 kHz.

So indeed, it is possible to modulate the intensity by modulating the input current of the laser over a large frequency range. This means that the diode module circuitry seen in Figure 22 and Figure 23 does not do anything to stabilize the output power of the laser against variations in the input power supply. Thus once other sources of noise decrease and laser intensity fluctuations become an issue, it will be a good idea to limit the noise of the input power supply into the laser as well. This might be important at the sites right now, but at the 40m other noise sources currently dominate.

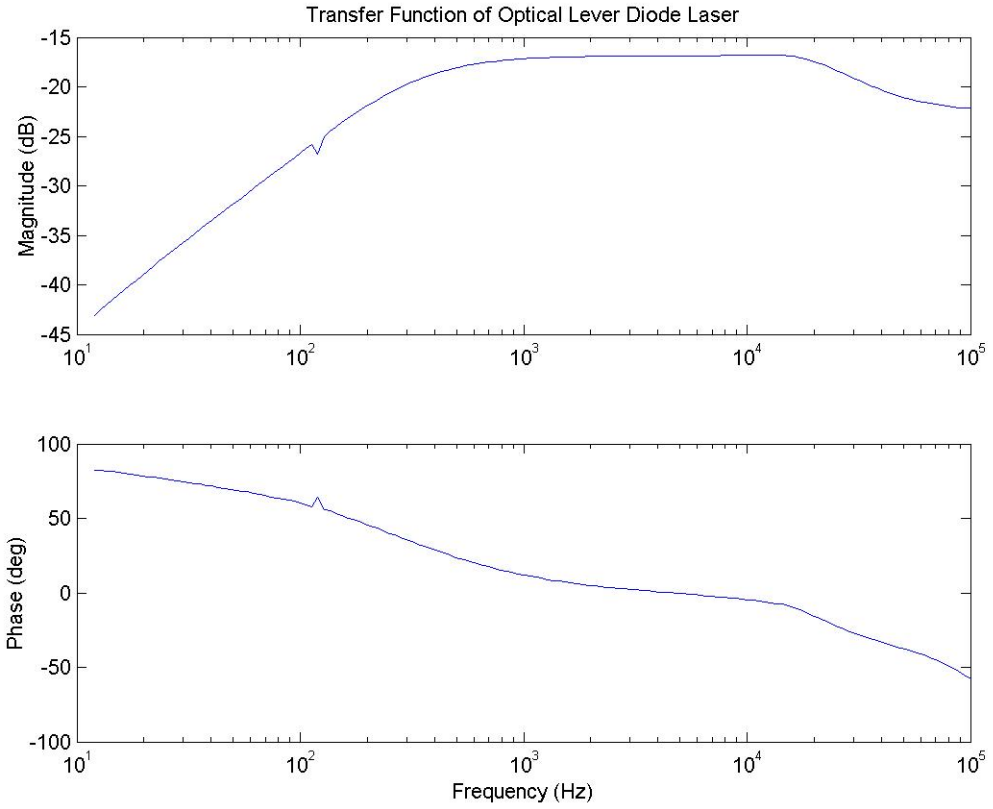

Figure 26: Transfer Function of Pin Voltage to Diode Power.

Optical Lever Noise Budget

Using all the calculated and calibrated sources of noise in the optical levers, a noise budget was created for when the DC readout scheme and output mode cleaner are in place. To do this, code was written to turn all the error signal data into tilts of the mirrors, then to output power at the asymmetric port (Appendix D), and finally to DARM signals (Appendix E) as seen in Figure 27.

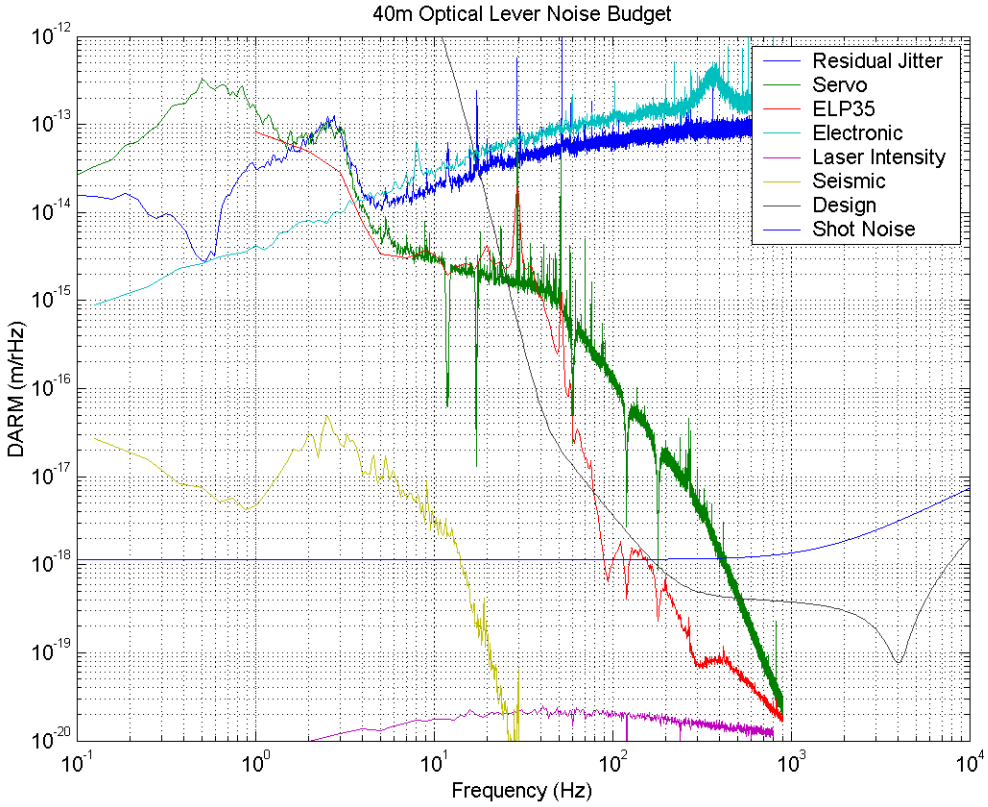

Figure 27: 40m Optical Lever Noise Budget for DC Readout with OMC.

The Residual Jitter curve represents the hypothetical DARM signal noise level from the apparent motion of the mirrors. However, above a few hertz this signal is dominated by the electronic noise so it does not represent the actual mirror motion, and thus does not represent an actual DARM signal. The noise from laser intensity also adds to the residual jitter though it does not represent true mirror motion. The electronic and laser intensity noise curves represent the DARM signals that would be seen if this noise indicated actual mirror motion. In contrast, the seismic noise curve determined from accelerometers on the ground does in fact indicate pendulum pitch motion of the mirrors leading to a DARM signal.

The actual optical lever noise floor is set by the residual jitter curve below about five hertz, and by the servo curve above five hertz. This is because the error signal measures mirror tilt accurately below a certain frequency though not above, while the servo signal tells what torque is being applied to the mirror through the coils and can be accurately converted to tilt of the mirrors above a certain frequency. Below a few hertz, the servo actively damps mirror motion, but above a certain frequency it basically just induces motion based on inaccurate error signals set by electronic and other sources of noise. Before the addition of the new ELP35 filter, the optical lever noise floor above five hertz was set by the green Servo curve. Now it has been significantly reduced as shown by the red ELP35 curve. This curve should be reduced even farther once whitening filters have been added to lower the base electronic noise along with the error signal on which the servo filters act. Optical lever noise could definitely stand to be reduced between five and a hundred hertz, and this is where the whitening filters should have the most effect. Below five hertz, the only way to improve detector sensitivity is to create servos that can more effectively damp mirror motion at those frequencies.

It appears that shot noise (calculated with 1 W input power and a 15pm offset) for the DC readout setup will be below the sensitivity level set by mirror motion up to 80 Hz, as calculated in Appendix F. Thus shot noise will set the noise floor above 80 Hz limiting the benefits gained from reducing optical lever noise above this frequency.

The design curve shown here is for the 40m with an input power of 100mW. (For the complete design sensitivity of the 40m, see Appendix G.) However, this study of the optical levers should prove useful in helping to reach the 40m interferometer's design sensitivity, and even provide insights into improving optical lever sensitivity at the sites.

Acknowledgments

I would like to thank my mentors Alan Weinstein and Rana Adhikari for all their help and support with this project. I would also like to thank the 40 m staff, LIGO, NSF, and the Caltech SURF program for making this work possible.

Appendix A: Optical Lever Calibration

To calibrate the oplev sensor signals from counts to radians of tilt of the mirrors, we proceed as follows. Lock the arm cavity (X or Y, in turn), with the mirror angular alignments adjusted for full power transmission as read out by the TRX or TRY photodiodes. The mirror tilts in pitch and yaw are read out by the oplev sensors. Then scan the mirror alignment (in pitch and yaw) by adjusting the bias slider on the suspension controller, observing the changing transmitted power and the changing oplev sensor reading. We use Reference 1 (Anderson) to relate the transmitted power to the absolute angular misalignment in radians, and thence to the oplev sensor reading in counts.

The paper by Dana Anderson can be used to determine the equation for power of a misaligned cavity. For each arm, a tilt of the initial flat test mass leads to an angular displacement of the cavity's axis. On the other hand, an angular displacement of the spherically curved end test mass leads to a translational displacement of the cavity's axis. In each case a power distribution results that is gaussian in the displacement of the axis. Knowing this distribution, it is possible to fit the power as a function of pitch and yaw and then map this onto the actual translational or angular displacement of the cavity axis.

The Perl script OplevCalibrationData.pl first restores and aligns the cavity (Appendix B). Then it scans through either pitch or yaw for a given test mass and prints out the corresponding time-averaged power and optical lever readings.

After that, Gaussian fits of the data for each test mass were used to find how the pitch and yaw translated to displacements of the cavity axis. Then these displacements were converted to the angular displacement of the mirror.

With the following relations:
pitch or yaw <=> cavity axis displacement;
cavity axis displacement <=> angular displacement of mirror;
pitch or yaw <=> optical lever reading,

it can be determined how the angular displacement of the mirror depends on the optical lever reading.

Here are the equations to carry out this calibration.

Electric field of beam along axis:

$$U_0 = \left(\frac{2}{\pi x_0^2}\right)^{1/4} \exp\left[-\left(\frac{x}{x_0}\right)^2\right]$$ where x_0 is the beam waist.

For translational displacement of axis,
the electric field of the beam in the misaligned cavity is:

$$\tilde{U}_0 = \left(\frac{2}{\pi x_0^2}\right)^{1/4} \exp\left[-\left(\frac{x-a_x}{x_0}\right)^2\right]$$

The power is proportional to the overlap of the two fields:

$$\Rightarrow P = \int_{-\infty}^{\infty} U_0(x) \bullet \tilde{U}_0(x) dx \propto \exp\left[-\frac{a_x^2}{2x_0^2}\right]$$

For angular displacement of axis,
the electric field of the beam in the misaligned cavity is:

$$\tilde{U}_0 = \left(\frac{2}{\pi x_0}\right)^{1/4} \exp\left[-\left(\frac{x}{x_0}\right)^2 + i\frac{2\pi\alpha_x x}{\lambda}\right]$$

$$\Rightarrow P = \int_{-\infty}^{\infty} U_0(x) \bullet \tilde{U}_0(x) dx \propto \exp\left[-\frac{\alpha_x^2 \pi^2 x_0^2}{2\lambda^2}\right]$$

I fit the power as a function of pitch or yaw with gaussian fits to find the mean and standard deviation of the data for the eight optical levers. Thus I obtained a_x and α_x in terms of the pitch and yaw readings.

After determining a_x and α_x, in both pitch and yaw directions, the angular displacement of the mirrors could easily be found with the following relations:

For the spherical mirrors (ETMX and ETMY), $a_x = R\sin\theta_x$, where R is the radius of the mirror. Thus if we know the pitch or yaw slider readout, we can calculate the tilt of a mirror in radians.

$$\Rightarrow \theta_x\left(a_{x\,pitch/yaw}\right) = \arcsin\left[\frac{1}{R} \cdot \left(a_x - \mu_{a_x}\right)_{pitch/yaw} \cdot \frac{x_0}{\sigma_{x_0\,pitch/yaw}}\right]$$

Then this tilt in radians can be plotted against the tilt of a mirror in perror or yerror counts. A linear fit of tilt in radians versus error signal gives the radians of tilt per count of oplev calibration.

For the flat mirrors (ITMX and ITMY), $\sin\alpha_x = \frac{\sin\theta_x}{1 - L/R}$, where L is the length of the arm cavity.

$$\Rightarrow \theta_x\left(\alpha_{x\,pitch/yaw}\right) = \arcsin\left[\left(1-\frac{L}{R}\right)\sin\left(\left(\alpha_x - \mu_{\alpha_x}\right)_{pitch/yaw} \cdot \frac{\lambda/\pi x_0}{\sigma_{\alpha_x\,pitch/yaw}}\right)\right]$$

For these calculations, the laser waist x_0 = 3.027mm, the laser wavelength λ = 1064 nm, the cavity length L = 38.250 m, and the radius of curvature of the spherical mirrors is R = 57.375 m (all obtained from the paper by Steve's desk). See example calculations for ITMY in Appendix C.

Here are the results giving the angle of deflection for each test mass:

ITMX pitch	65 μrads/count of oplev
ITMX yaw	57 μrads/count
ETMX pitch	142 μrads/count
ETMX yaw	213 μrads/count

ITMY pitch	111 μrads/count
ITMY yaw	92 μrads/count
ETMY pitch	218 μrads/count
ETMY yaw	248 μrads/count

The optical levers for the ITMs are over twice as sensitive because their optical path lengths, i.e. lever arms, are substantially longer than for the ETMs. The optical levers for the ETMs are on benches that are much closer to the test masses.

This calibration will be quite important for reducing noise and keeping the interferometer locked once the new DC readout system is in place. For that we will need to know more accurately the angular changes of the mirrors, as determined from the calibrated optical lever readings.

Appendix B: Perl Script "OplevCalibrationData.pl"

In the future, to be located at /cvs/cds/caltech/users/Royal/OplevCalibrationData.pl
Until I get back to Caltech, at /cvs/cds/caltech/users/Royal/TakeData.pl

```
#!/usr/bin/perl -w

use strict;

#  Initialize values from the command line

my $arm = $ARGV[0];         # "X" or "Y";
my $mirror = $ARGV[1];      # "E" or "I";
my $tilt = $ARGV[2];        # "PIT" or "YAW"
print $arm."\n";
print $mirror."\n";
print $tilt."\n";

#  Construct name of optical lever channel

my $ifo = "C1";
my $mname = $mirror."TM".$arm;
my $dof = &name($tilt);

sub name{
    if ($tilt eq "PIT") {
        my $dof = "PITCH";
    } elsif ($tilt eq "YAW") {
        my $dof = "YAW";
    } else {
        print "Bad DOF name.:  ".$dof."\n";
    }
}

my $olname = $ifo.":SUS-".$mname."_OL_".$dof;

#  Construct name of test mass channel
#  (the one from which to read/write the pitch or yaw)

my $tmchname = $ifo.":SUS-".$mname."_".$tilt."_COMM";

#  Construct name of channel to read power from

my $pchname = $ifo.":LSC-TR".$arm."_OUT16";

print "pchname is ".$pchname."\n";



#  Restore mirror

system "/cvs/cds/caltech/burt/c1ifoconfigure/C1configure".$arm."arm";

#  Align mirror

system "/cvs/cds/caltech/scripts/AutoDither/medm/medmAlign".$arm;

sleep 5;

# Wait in this while loop until the Autodither is done
my $bit = `/cvs/cds/caltech/scripts/general/pezcabit C1:IFO-STATE 5 TEST`;
while ($bit == 1){
       sleep 6;
       print "Still auto-dithering...\n";
       $bit = `/cvs/cds/caltech/scripts/general/pezcabit C1:IFO-STATE 5 TEST`;
}
print "Finished alignment\n";


# Private Variables

my $maxPower = `tdsread $pchname`;    # Read from channel
print "maxPower is ".$maxPower."\n";
my $tiltAtMax = `tdsread $tmchname`;  # Read from channel
#my $tiltAtMax = -1.9;
print "tiltAtMax is ".$tiltAtMax."\n";
my $powerBound = .8 * $maxPower;
```

```
print "powerBound is ".$powerBound."\n";
my $powerVal = $maxPower;
print "powerVal is ".$powerVal."\n";
my $tiltVal = $tiltAtMax;

# Move from center of peak to a lower bound
while ($powerVal > $powerBound) {
    `tdswrite $tmchname $tiltVal`;  # Write to channel
    sleep 1.5;
    $powerVal = `tdsavg 2 $pchname`; # Read from channel
    print "powerVal is ".$powerVal;
    # Decrement the tilt Value
    $tiltVal = $tiltVal - .01;
}
# Now tiltVal is at its lower bound

print "here\n";

#  Private Variables

my $tiltLb = $tiltVal;
print "tiltLb is ".$tiltLb."\n";
my $tiltDiff = $tiltAtMax - $tiltLb;
print "tiltDiff is ".$tiltDiff."\n";
my $tiltUb = $tiltAtMax + $tiltDiff+.03;
print "tiltUb is ".$tiltUb."\n";

# Record power over range of values from lower to upper bound of tilt

while ($tiltVal < $tiltUb) {
    `tdswrite $tmchname $tiltVal`;  # Write to channel
    sleep 1.5;
    my @data = `tdsavg 2 $pchname $olname`;  # Read from channel
    chomp($powerVal = $data[0]);
    chomp(my $oplevVal = $data[1]);
    # Print the tilt, the power, and the oplev value
    print $tiltVal;
    print "\t";
    print $powerVal;
    print "\t";
    print $oplevVal;
    print "\n";
    # Increment the tilt value
    $tiltVal = $tiltVal + .01;
}

#Return to initial aligned tilt

my $middleTilt = $tiltLb + $tiltDiff;
`tdswrite $tmchname $middleTilt`;
```

Appendix C

In Figure 28, we see how the mean and standard deviation of cavity axis tilt can be found.

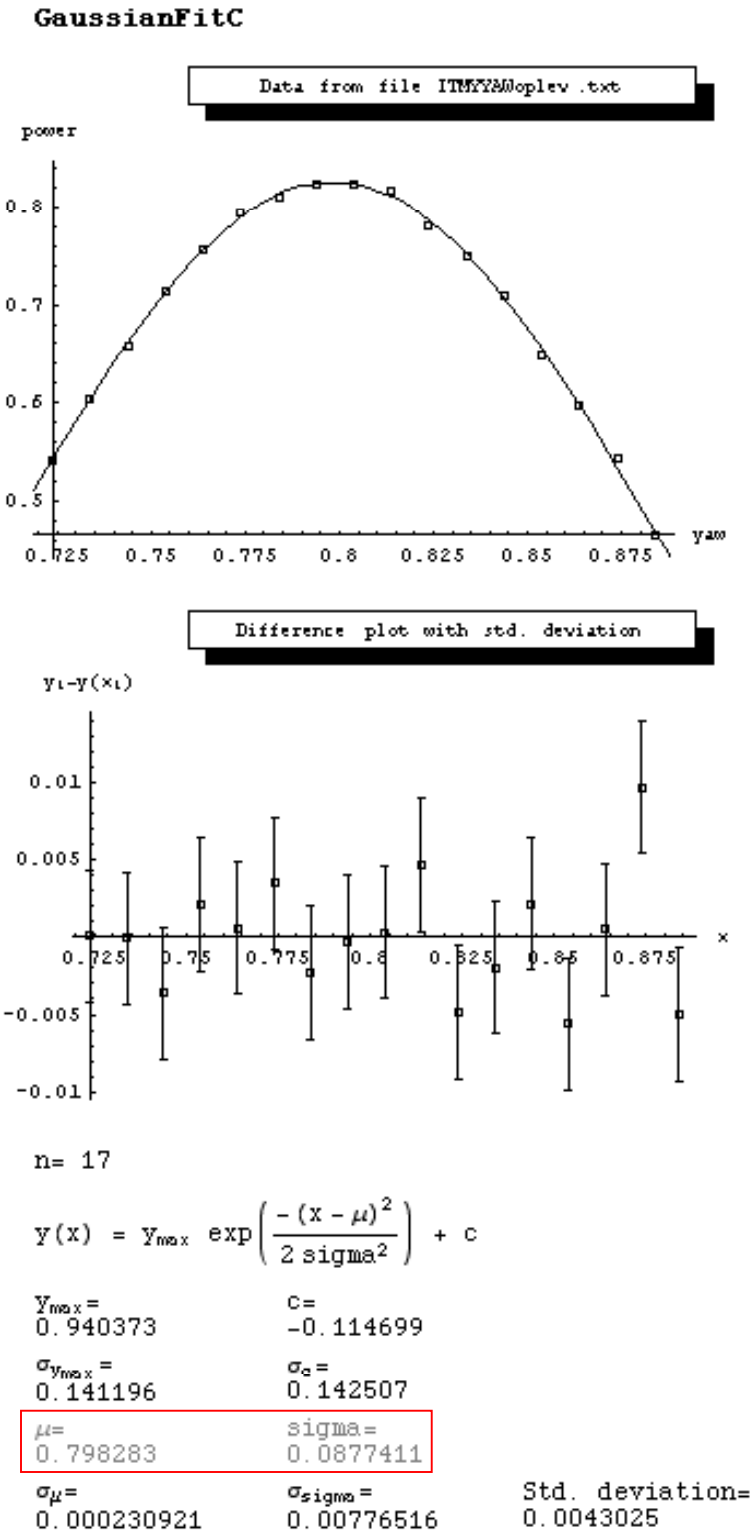

Figure 28: Gaussian fit of power to yaw for the ITMY.

Figure 29 shows the raw yaw signals plotted against the yerror signal for the ITMY mirror. Below the plot, the yaw signal is converted to the tilt of the mirror using the formula in Appendix A for a flat mirror, along with the mean and standard deviation from the Gaussian fit of power as a function of yaw. Symbolically this calculation is given by:

$$\text{ynew} = \theta_x\left(\alpha_{x\,pitch/yaw}\right) = \arcsin\left[\left(1-\frac{L}{R}\right)\sin\left(\left(\alpha_x-\mu_{\alpha_x}\right)_{pitch/yaw}\cdot\frac{\lambda/\pi x_0}{\sigma_{\alpha_x\,pitch/yaw}}\right)\right]$$

(In the equations in the figure, x and xnew refer to the yerror signal, while y refers to the yaw signal and ynew refers to the calculated tilt in radians of the ITMY in the yaw direction.)

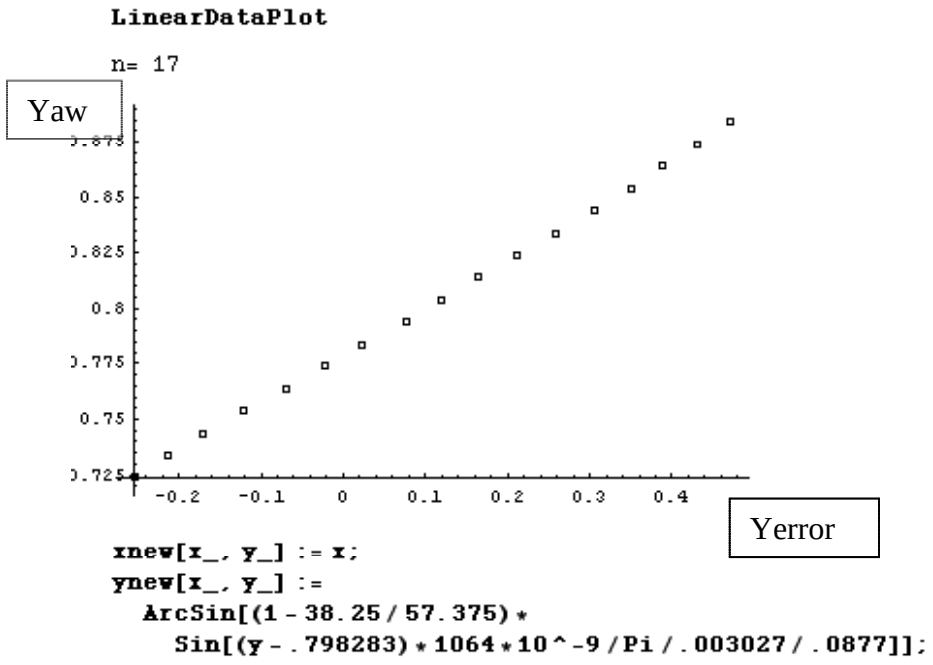

Figure 29: Plot of Yaw Reading versus Yerror for ITMY

Figure 30 shows the linear fit of calculated mirror tilt in radians to the actual yerror signal in counts. Thus the slope, b, of the line give the final calibration factor of radians per count of the oplev sensor for ITMY yaw tilt.

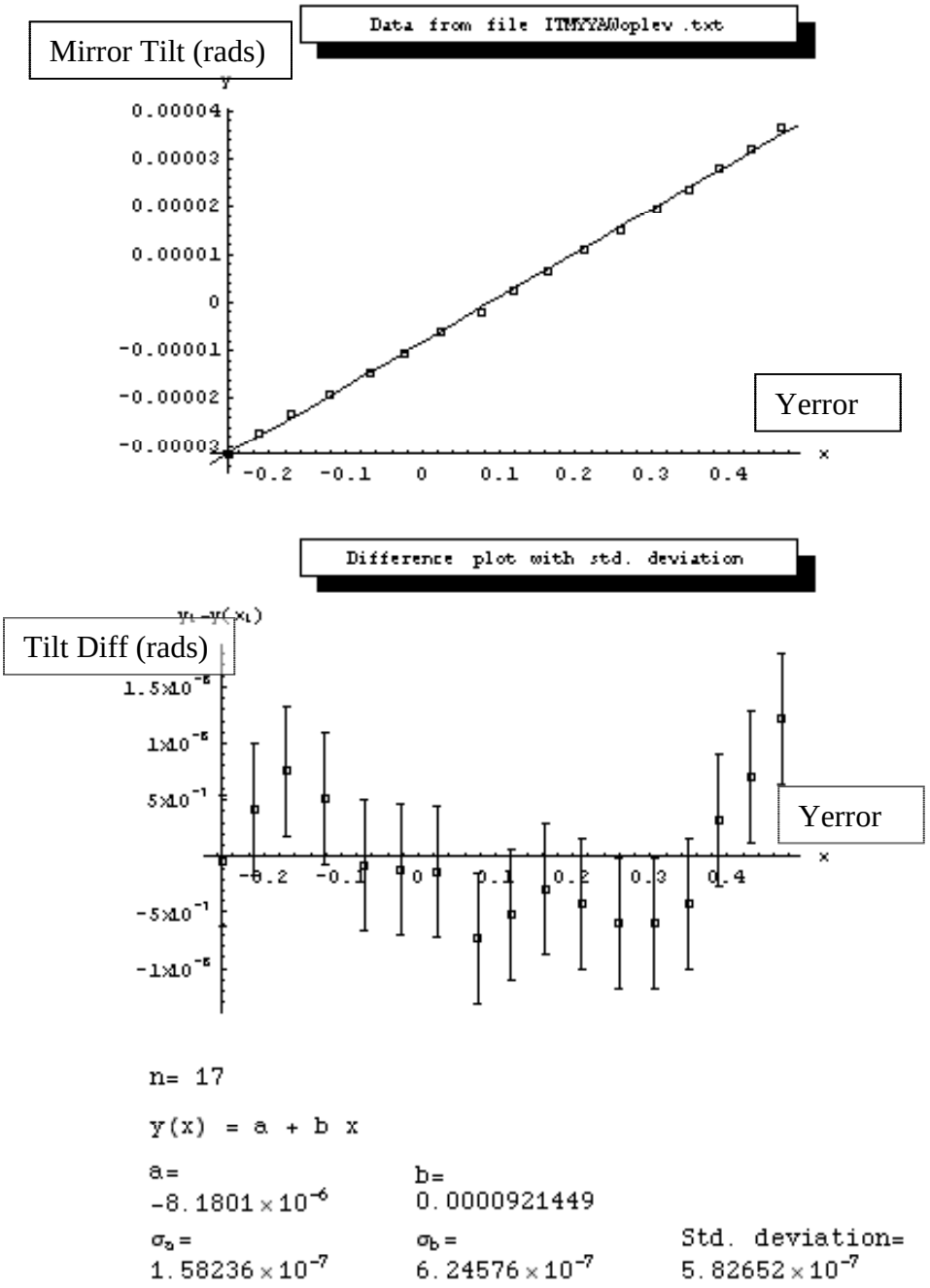

Figure 30: Linear Fit of Mirror Tilt to Yerror reading for ITMY

Appendix D: Calculation of power at OMC

Now that I have this jitter data, I must determine how it translates to the power in the output mode cleaner (OMC). The beam that comes out of the arm cavity gets transformed by a beam reducing telescope (BRT) on the way to the OMC. To do this I am using ray matrices. Here is a schematic diagram of the setup:

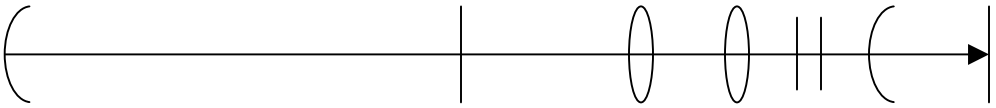

40m arm cavity d_1=2m 4x BRT d_2 OMC

This can be described mathematically by:

$$\begin{vmatrix} a_{xOMC} \\ \alpha_{xOMC} \end{vmatrix} = \begin{vmatrix} 1 & d_2 \\ 0 & 1 \end{vmatrix} \begin{vmatrix} 1/4 & 0 \\ 0 & -4 \end{vmatrix} \begin{vmatrix} 1 & d_1 + 40m \\ 0 & 1 \end{vmatrix} \begin{vmatrix} a_{xETM} \\ \alpha_{xETM} \end{vmatrix},$$

where $a_{xETM} = a_x$ and $\alpha_{xETM} = \alpha_x$ as determined from the optical lever readings. This will lead to translational and angular deflections from the OMC cavity axis of the beam going into the OMC in two orthogonal directions. The overall translation is $a_{OMC} = \sqrt{a_{xOMC}^2 + a_{yOMC}^2}$, and assuming small angles, the overall tilt is $\alpha_{OMC} = \sqrt{\alpha_{xOMC}^2 + \alpha_{yOMC}^2}$.

What I need to do now is take the translation and tilt jitter data in both directions, ie $\theta_{initial}$ and apply the transfer function of the servo to get $\theta(f) = \left| \frac{\theta_{initial}}{1 + G(f)} \right|$. The gain comes from two flat mirrors that are used to steer the beam into the mode cleaner.

Then the power as a function of translation is proportional to (1- $a_{OMC}^2 / 2x_0^2$) and as a function of tilt is proportional to (1- $\frac{\alpha_{OMC}^2 \pi^2 x_0^2}{2\lambda^2}$). Thus the total power seen at the OMC will be the sum in quadrature of the two varying parts of each of these functions which is $\sqrt{\left(\frac{a_{OMC_{RMS}} \bullet a_{OMC}(f)}{2x_0^2} \right)^2 + \left(\frac{\alpha_{OMC_{RMS}} \bullet \alpha_{OMC}(f)}{2\lambda^2 / \pi^2 x_0^2} \right)^2}$, assuming the incident power in on the order of one watt.

NOTE: Now I'm not sure if these equations are right since in my calculations, I used the same laser waist from the arm cavities (3.027 mm). It seems that I should now use the waist for the OMC cavity but I don't know what this is.

Appendix E: Calculation of Equivalent DARM Signals for DC Readout

For homodyne detection of gravitational waves using a Michelson Interferometer with Fabry-Perot arm cavities, the power at the asymmetric port depends on the length difference between the two arms. This length difference is the sum of a deliberate offset Δ (about 10 pm at the 40 m) between the arms plus small variations dL in length due to noise or gravitational waves.

The electric field at the asymmetric port is given by:

$$E_{AS} = E_{inc} t_{bs} r_{bs} \left[e^{i2\phi} \left(\frac{r_1 - r_2 e^{-2ikL_x}}{1 - r_1 r_2 e^{-2ikL_x}} \right) - e^{i2\phi} \left(\frac{r_1 - \tilde{r}_2 e^{-2ikLy}}{1 - r_1 \tilde{r}_2 e^{-2ikLy}} \right) \right]$$

The two different end reflectivities simulate round trip losses of 200 ppm in the cavity.

We can rewrite the electric field at the asymmetric port with L_x=-Δ/2-dL/2 and L_y=Δ/2+dL/2 as:

$$E_{AS}(dL) = E_{inc} t_{bs} r_{bs} \left[e^{i2\phi} \left(\frac{r_1 - r_2 e^{-2ik(-\Delta/2 - dL/2)}}{1 - r_1 r_2 e^{-2ik(-\Delta/2 - dL/2)}} \right) - e^{i2\phi} \left(\frac{r_1 - \tilde{r}_2 e^{-2ik(\Delta/2 + dL/2)}}{1 - r_1 \tilde{r}_2 e^{-2ik(\Delta/2 + dL/2)}} \right) \right]$$

Since homodyne detection uses the carrier light as the local oscillator, the power as a function of length at the asymmetric port is given by:

$$P_{AS}(dL) = E_{AS}^{*}(dL) \cdot E_{AS}(dL)$$

This can be Taylor Expanded in dL about 0 to get an approximate expression for the power at the asymmetric port:

$$P_{AS}(dL) \approx P_{AS}(0) + dL \cdot P'_{AS}(0),$$

From there we obtain the DARM signal dL as a function of the power fluctuations and the derivative of the power at the deliberate offset.

$$\Rightarrow dL \approx \left(P_{AS}(dL) - P_{AS}(0) \right) / P'_{AS}(0)$$

This result of this calculation is in the code DCdarmlossy.m

Appendix F: Shot Noise Calculation

The DARM signal due to shot noise can be approximated (from Rana's thesis):

$\approx \frac{\sqrt{\frac{2hc}{\lambda} P_{AS}(\Delta)}}{dP/dL|_{\Delta}} \cdot \left(1 + i\frac{f}{f_c}\right)$, where Δ is the deliberate offset for the DC readout detection, and $f_c = \frac{c/2L}{2F}$

The finesse of the arms F = 1235.
Cavity length L = 38.55 m.
Deliberate offset Δ = 200 pm was found to have the best signal to noise ratio from the following calculations, assuming 1 watt of incident power.

```
tbs = Sqrt[.5];
rbs = Sqrt[.5];
t1 = 1 - r1;
t2 = 1 - r2;
r1 = .995;
r2 = .99999;
r2a = .95*r2;
lambda = 1064*10^-9;
k = 2*Pi/lambda;
delta = 2*10^-10;
```

In[210]:=
```
powerlinlossy[dL_] =
  tbs^2*rbs^2*
   ((r1 - Exp[-2*I*k*(-dL/2)]*r2)/(1 - Exp[-2*I*k*(-dL/2)]*r1*r2)
     + (r1 - Exp[-2*I*k*(dL/2)]*r2a)/(1 - Exp[-2*I*k*(dL/2)]*r1*r2a))*
   ((r1 - Exp[2*I*k*(-dL/2)]*r2)/(1 - Exp[2*I*k*(-dL/2)]*r1*r2) +
     (r1 - Exp[2*I*k*(dL/2)]*r2a)/(1 - Exp[2*I*k*(dL/2)]*r1*r2a));
```

In[211]:=
```
powerapprox[dL_] := powerlinlossy[0] + dL*powerlinlossy'[0] +
   dL^2/2*powerlinlossy''[0];
```

In[212]:=
```
powerapproxderiv[dL_] := powerlinlossy'[0] + dL*powerlinlossy''[0];
```

In[213]:=
```
Plot[Abs[powerapprox[dL]], {dL, -1*10^-9, 1*10^-9}]
```

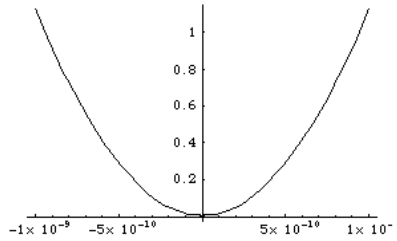

Out[213]= - Graphics -

In[214]:=
```
Plot[Abs[powerlinlossy[dL]], {dL, -1*10^-9, 1*10^-9}]
```

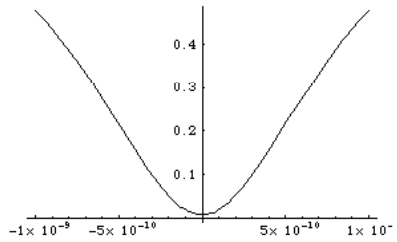

Out[214]= - Graphics -

In[215]:=
```
powerlinderivlossy[dL_] = powerlinlossy'[dL];
```

In[216]:=
```
powerlinapprox[dL_] := powerlin[delta] + dL*powerlinderiv[delta]
```

In[217]:=
```
SNR[dl_] := powerlinderivlossy[dl] / Sqrt[powerlinlossy[dl]];
```

In[218]:=
```
Plot[SNR[dl], {dl, -1*10^-10, 3*10^-10}]
```

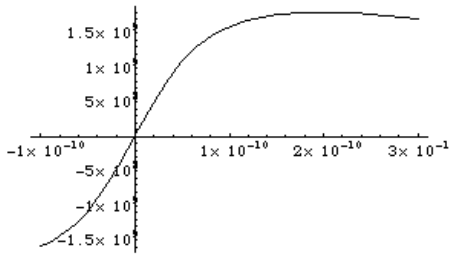

Out[218]= - Graphics -

In[219]:=
```
SNRapprox[dl_] := powerapproxderiv[dl] / Sqrt[powerapprox[dl]];
```

In[234]:=
```
Plot[SNRapprox[dl], {dl, -1*10^-10, 3*10^-10}]
```

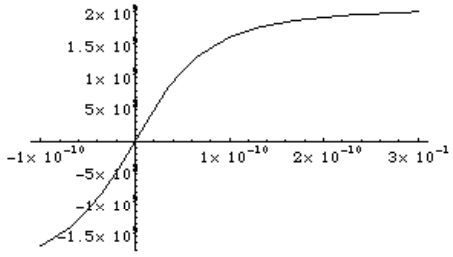

Out[234]= - Graphics -

In[221]:=
```
h = 6.626 *10^-34;
c = 3*10^8;
L = 38.55;
F = 1235;
lambda = 1064*10^-9;
k = 2*Pi / lambda;
phi = delta*k;
```

In[228]:=
```
fc = c / (2*L*2*F);
```

In[229]:=
```
Abs[powerapprox[delta]]
```

Out[229]= 0.0521653

In[230]:=
```
Abs[powerapproxderiv[delta]]
```

Out[230]= 4.45904×10^{8}

In[235]:=
```
Shot[f_] :=
 Abs[Sqrt[h*c / lambda*powerapprox[delta]] / powerapproxderiv[delta]*(1 + I*f / fc)]
```

In[232]:=
```
Plot[Shot[f], {f, 0, 10000}]
```

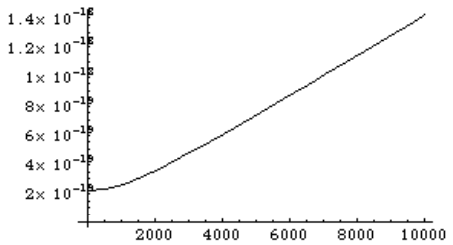

Out[232]= - Graphics -

Appendix G: Sensitivity Design Curve for the 40m Interferometer.

Figure 31 shows the theoretical contributions to the 40m design sensitivity curve from fundamental noise sources.

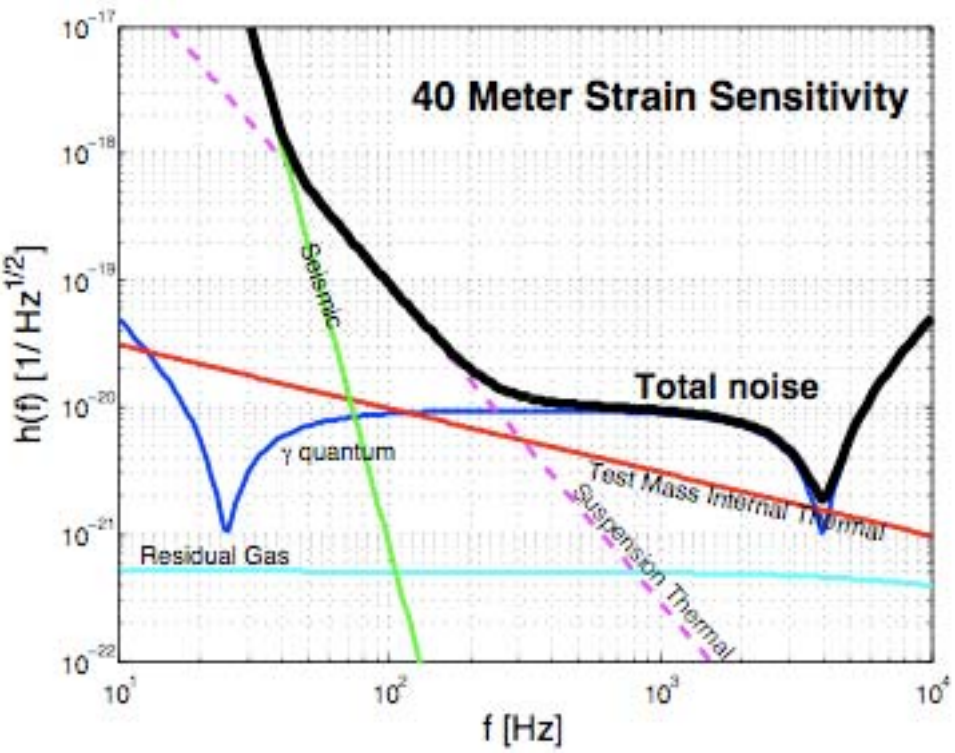

Figure 31: 40m Design Sensitivity

Reference

1. Anderson, Dana Z. "Alignment of resonant optical cavities." *Applied Optics*. Vol. 23, No. 17. 1 Sept. 1984.